



universität
wien

DIPLOMARBEIT

Titel der Diplomarbeit

Investigation of the σ -to- α -phase transition in
FeCr

Verfasserin

Alice Mikikits-Leitner

angestrebter akademischer Grad

Magistra der Naturwissenschaften (Mag. rer. nat.)

Wien, im September 2009

Studienkennzahl lt. Studienblatt: A 411
Studienrichtung lt. Studienblatt: Physik
Betreuer: ao. Univ.-Prof. Bogdan Sepiol

Abstract

The goal of this thesis was to investigate the σ -to- α -phase transition in the system iron-chromium (Fe-Cr). This was done by means of ex-situ ^{57}Fe Mößbauer spectroscopy, which provided a well-suited tool to distinguish between the two phases, since the σ -phase is paramagnetic at room temperature whereas the high-temperature α -phase is ferromagnetic.

We isothermally annealed samples of two different compositions, namely $\text{Fe}_{51}\text{Cr}_{49}$ and $\text{Fe}_{53.8}\text{Cr}_{46.2}$, at various temperatures above the critical temperature of 821°C . In that way we gained information about the kinetics of the phase transition in terms of the Johnson-Mehl-Avrami-Kolmogorov-equation.

From the obtained values for the Avrami exponent conclusions about the type of nucleation mechanism could be drawn. The Avrami exponent varied between 1 for temperatures near the critical temperature and 4 for higher temperatures. That indicated that the nucleation mechanism changes from heterogeneous to homogeneous.

Moreover, an effective activation energy of $E = 10.57 \pm 0.92$ eV (1020 ± 88 kJ/mol) could be determined.

Apart from that we observed a phenomenon which seems to have never been observed until now; namely that the orientation of the axis of magnetization is a function of the α -fraction present in the sample. It changes from “out-of-plane” to “in-plane” as the α -amount increases.

Zusammenfassung

Das Ziel dieser Diplomarbeit war es, den σ -zu- α -Phasenübergang im Legierungssystem Eisen-Chrom (Fe-Cr) zu untersuchen. Dies wurde mittels ex-situ ^{57}Fe Mößbauer Spektroskopie bewerkstelligt, die eine geeignete Methode darstellt zwischen den zwei Phasen zu unterscheiden, da die σ -Phase paramagnetisch bei Raumtemperatur und die Hochtemperatur- α -Phase ferromagnetisch ist.

Durch Auslagern von Proben unterschiedlicher Zusammensetzung, nämlich $\text{Fe}_{51}\text{Cr}_{49}$ und $\text{Fe}_{53.8}\text{Cr}_{46.2}$, bei verschiedenen Temperaturen über der kritischen Temperatur von 821°C erhielten wir Informationen über die Kinetik des Phasenübergangs mittels der Johnson-Mehl-Avrami-Kolmogorov Methode.

Von den ermittelten Werten für den Avrami-Exponenten konnten wir Rückschlüsse über den Typ des Nukleationsmechanismus ziehen. Der Avrami-Exponent variierte zwischen 1 für Temperaturen nahe der kritischen Phasenübergangstemperatur und 5 für höhere Temperaturen. Das bedeutet, dass der Nukleationsmechanismus mit zunehmender Temperatur von heterogen zu homogen wechselt.

Darüber hinaus konnten wir eine effektive Aktivierungsenergie von $E = 10.57 \pm 0.92$ eV (1020 ± 88 kJ/mol) bestimmen.

Abgesehen davon haben wir ein Phänomen beobachtet, welches bis jetzt nicht bekannt zu sein scheint; die Orientierung der Hauptachse der Magnetisierung ist eine Funktion vom α -Anteil in der Probe. Sie wechselt mit zunehmendem α -Anteil von "out-of-plane" zu "in-plane".

Acknowledgements

First I want to express my gratitude to my thesis supervisor Bogdan Sepiol. The subject of this thesis which he suggested to me turned out to be a very interesting one. Moreover, his competence in this field and his cooperation concerning the experimental measurements turned out to be an indispensable support for me.

I would like to take this opportunity to thank the people of the group “Dynamics of Condensed Systems” at the Faculty for Physics, which ensured me good working conditions and a pleasant atmosphere.

Moreover, I want to thank Jakub Cieślak from the University of Mining and Metallurgy (AGH), Poland. He provided the samples for the measurements and gave specialized advice.

My greatest thanks are due to my husband Michael, who was an important person to ask for support concerning physical questions. The very critical but helpful and fruitful discussions about the subject helped me all the time while working on my thesis. But most of all I want to thank him for his love, patience, and for being always on my side.

Finally I want to say thanks to my parents who always believed in me and are showing respect for what I am doing although they may never understand much about the subject.

Danksagung

Als Erstes gebührt mein Dank meinem Diplomarbeitsbetreuer Bogdan Sepiol. Das Thema meiner Diplomarbeit, welches er mir vorgeschlagen hat, stellte sich als äußerst interessant heraus. Darüber hinaus waren seine fachlichen Kompetenzen und seine Mitwirkung bei den experimentellen Messungen eine für mich unverzichtbare Hilfe.

Ich möchte diese Gelegenheit nutzen um allen Leuten der Gruppe „Dynamik Kondensierter Systeme“ der Fakultät für Physik für die guten Arbeitsbedingungen und die angenehme Atmosphäre innerhalb der Gruppe zu danken.

Des Weiteren bedanke ich mich bei Jakub Cieślak von der Universität für Bergbau und Metallurgie (AGH), Polen. Er stellte die Proben zur Verfügung und gab fachlichen Rat.

Mein größter Dank gilt meinem Ehemann Michael, der eine wichtige Ansprechperson bezüglich physikalischer Fragestellungen darstellte. Während der Arbeit an dieser Diplomarbeit haben mir die sehr kritischen aber äußerst hilfreichen und fruchtbaren Diskussionen über das Thema sehr geholfen. Am meisten jedoch danke ich ihm für seine Liebe, Geduld und dafür, dass er immer an meiner Seite ist.

Zu guter Letzt sage ich meinen Eltern Danke dafür, dass sie immer an mich geglaubt haben und Respekt für meine Arbeit zeigen, obwohl sie wahrscheinlich nie viel davon verstehen werden.

Contents

1	Introduction	1
2	Möbbaauer spectroscopy	3
2.1	Möbbaauer effect	3
2.1.1	Recoil-free fraction and Lamb–Möbbaauer factor	5
2.1.2	Natural linewidth	6
2.2	Hyperfine interactions	8
2.2.1	Chemical isomer shift	8
2.2.2	Electric quadrupole interactions	9
2.2.3	Magnetic hyperfine interactions	10
2.2.4	Relative intensities of absorption lines	11
3	Phase transformations	13
3.1	Theory of nucleation	13
3.1.1	Critical nucleus	13
3.1.2	Heterogeneous nucleation	14
3.2	Kinetics of phase transformations	16
3.2.1	The Kolmogorov-Johnson-Mehl-Avrami equation	16
4	Experimental details	19
4.1	The Möbbaauer spectroscopy equipment	19
4.1.1	Source	19
4.1.2	Electronics of the Möbbaauer spectrometer	19
4.1.3	Calibration	21
4.2	Preparation and treatment of the samples	21
4.2.1	Preparation of the samples	22
4.2.2	Treatment of the samples	22
5	The system iron-chromium	23
5.1	The σ -phase	24
5.2	The α -phase	27
5.3	The σ -to- α phase transition	28
6	Results	31
6.1	Fitting procedure and evaluation of the transmission spectra	31
6.2	Kinetics of the phase transformation	38
6.2.1	Activation energy	38

Contents

6.2.2	Avrami-Exponent	43
6.2.3	Relative intensities of the absorption lines	44
6.2.4	Mean magnetic field	45
7	Summary and conclusion	47
	Bibliography	49
	Curriculum vitae	53

1 Introduction

The system iron-chromium (Fe-Cr) has always attracted the attention of scientists (especially physicists) and industrial researchers. This stems from the fact that Fe-Cr is the base-alloy of stainless steel, an indispensable material in industry as well as in everybody's day-to-day life.

Ferritic stainless steels are alloys of various elements such as iron, chromium, molybdenum, nickel, aluminium, and titanium. Such steels show a high-temperature corrosion resistance, but degrade by formation of the σ -phase. The latter is also apparent in many binary and ternary iron-alloy systems, e.g. Fe-Cr, Fe-V, and Fe-Mo. The σ -phase is hard and brittle and significantly deteriorates the properties of stainless steels.

This explains the outstanding interest in the formation and growth of the σ -phase in stainless steels but also in Fe-Cr since it is a well-defined model system. The phase transition from ferrite (bcc) into the σ -phase in duplex stainless steels was investigated in [Elmer07] by in-situ synchrotron X-ray diffraction methods. In [Cieślak99], [Blachowski99], and [Blachowski00a] Cieślak et al. studied the kinetics of the σ -phase formation in iron-chromium doped with various amounts of titanium or aluminium in order to understand the influence of these alloying elements, which are, as above mentioned, main constituents of stainless steels. They did their investigations by means of in-situ ^{57}Fe Mößbauer spectroscopy.

Especially ^{57}Fe Mößbauer spectroscopy turns out to be a suitable tool to study phase transitions in an Fe-doped alloy. Mößbauer spectroscopy is based on the resonant emission and absorption of γ -rays without energy loss due to recoil. This effect is called the Mößbauer effect. Mößbauer spectroscopy has a high resolution in the energies of the nuclear states. This makes it possible to observe changes in the nuclear environment of the atom in the solid. Such hyperfine interactions are the chemical isomer shift, the electric quadrupole splitting, and the magnetic hyperfine structure.

In other words, by Mößbauer spectroscopy one can study phase transitions by observing the difference in the hyperfine interactions in two phases. In the case of Fe-Cr the α -phase is ferromagnetic whereas the σ -phase is paramagnetic.

In this thesis we will study the σ -to- α -phase transition by ex-situ ^{57}Fe Mößbauer spectroscopy. The content of the thesis will be structured in the following way.

Chapter 2 describes the Mößbauer effect in detail as well as the hyperfine interactions made measurable by Mößbauer spectroscopy. An introduction into Mößbauer spectroscopy as an important spectroscopic technique with a wide range of applications is given.

Chapter 3 deals with the theory of phase transformations. A brief overview of the theory of phase transitions happening via nucleation and growth mechanisms is

1 Introduction

presented. Moreover, concerning the kinetics of such a phase transformation, the Johnson-Mehl-Avrami-Kolmogorov-equation will be derived as a tool to describe the temporal evolution of a phase transition.

Chapter 4 deals with the experimental setup and procedures. A description of the Mößbauer spectroscopy equipment, i.e., of the source and the electronics of the spectrometer is given.

Moreover information about the way the samples were prepared and treated during experimentation is given.

Chapter 5 is devoted to the system iron-chromium. The structure and properties of the two phases, the σ - and α -phase, are described. Finally, concerning the kinetics of the σ -to- α -phase transition, two possibilities for determining the α -fraction from the Mößbauer spectra are discussed.

Chapter 6 presents the results of the measurements and their interpretation. The fitting procedure and evaluation of the transmission spectra is discussed in great detail. From the results concerning the temporal evolution of the phase transition at various temperatures and for different compositions we obtain information about the nucleation mechanism happening during the transformation. Moreover a value for the effective activation energy is given. Observations on the dependence of the mean magnetic field and the preferred orientation of magnetization on the α -fraction in the sample are made.

Chapter 7 finally compiles all results and conclusions which could be derived from the investigation of the σ -to- α -phase transition.

2 Mößbauer spectroscopy

In this chapter we want to discuss Mößbauer spectroscopy, a spectroscopic technique which relies on a physical phenomenon called the Mößbauer effect, which was first discovered by Rudolf Mößbauer (1957). Only two years later (1961) he was awarded the Nobel Prize in Physics for his discovery, since it soon turned out to have a deep impact on scientific, in particular physical, research.

The main references for this chapter are [Greenwood71] and [Wegener66]. Both describe the Mößbauer effect and its wide range of application in different areas of scientific research in a clear way.

2.1 Mößbauer effect

The Mößbauer effect is the emission and absorption of γ -rays without loss of energy due to recoil.

Let us first consider a single atom of mass M , which moves with a velocity \vec{V} . This atom can be in the ground state corresponding to the energy E_g or in an excited state with the energy E_e . The energy difference between the ground state E_g and excited state E_e is given by

$$E_0 = E_e - E_g.$$

In the case where the atom is in an excited nuclear state there can happen a nuclear transition from this state to the ground state. Before the nuclear transition the total energy of the nucleus is $E_0 + \frac{1}{2}M\vec{V}^2$. During the transition from the excited to the ground state a photon is emitted, which has the energy E_γ . After the emission of the γ -ray the initial velocity of the atom is modified. The velocity of the atom after emission is then given by $\vec{V} + \vec{v}$. Thus the total energy of the system after emission is given by $E_\gamma + \frac{1}{2}M(\vec{V} + \vec{v})^2$. Due to energy conservation we get

$$E_0 + \frac{1}{2}M\vec{V}^2 = E_\gamma + \frac{1}{2}M(\vec{V} + \vec{v})^2.$$

Hence the difference between the energy of the γ -ray E_γ and the energy of the nuclear transition E_0 is given by

$$E_0 - E_\gamma = \frac{1}{2}M\vec{v}^2 + M\vec{v}\vec{V}. \quad (2.1)$$

The first term in equation (2.1) is the so-called recoil kinetic energy $E_R = \frac{1}{2}M\vec{v}^2$ and the second term is the Doppler-effect energy $E_D = M\vec{v}\vec{V}$. In other words, equation (2.1) tells us that the γ -ray energy is not equal to the energy of the nuclear transition, rather it is modified by recoil and the Doppler-effect.

2 Mößbauer spectroscopy

Let us denote the recoil momentum of the atom by \vec{Q} and the one of the γ -ray photon by \vec{Q}_γ . The recoil kinetic energy can then be written as

$$E_R = \frac{1}{2}M\vec{v}^2 = \frac{\vec{Q}^2}{2M}. \quad (2.2)$$

Due to momentum conservation we have

$$\vec{Q} + \vec{Q}_\gamma = 0.$$

Thus we obtain

$$\vec{Q} = -\vec{Q}_\gamma = -\frac{E_\gamma}{c} \quad (2.3)$$

and finally by inserting this expression into (2.2) yields

$$E_R = \frac{E_\gamma^2}{2Mc^2}. \quad (2.4)$$

Next, we will discuss gamma resonance emission and absorption of free atoms at rest ($V = 0$), cf. Figure 2.1. If we consider a nucleus emitting a γ -ray photon, the energy of the later E_γ is decreased due to recoil of the nucleus, that is $E_\gamma = E_0 - E_R$. Consider now the reverse process, where this γ -ray is reabsorbed by another nucleus. The necessary energy, which should be transferred to the absorbing nucleus, such that it gets excited is given by $E_0 + E_R$.

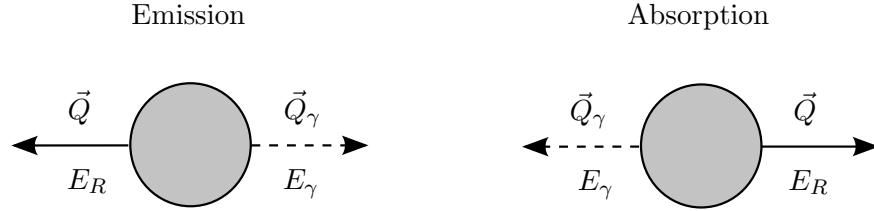


Figure 2.1: Emission and absorption of a γ -ray photon.

Quantum mechanics tells us that an excited state E_1 of an atom is not given by a sharply defined energy difference E_0 to the ground state E_g , rather it is described by an energy probability distribution $I(E)$ centered at E_0 (cf. Section 2.1.2, equation (2.10)). Let us denote the linewidth of this distribution by Γ_0 . The fact described above has the major consequence that free-atom nuclear resonance happens only where emission- and absorption line overlap. If we take a look at Figure 2.2 we conclude that this leads to the requirement

$$2E_R \lesssim \Gamma_0.$$

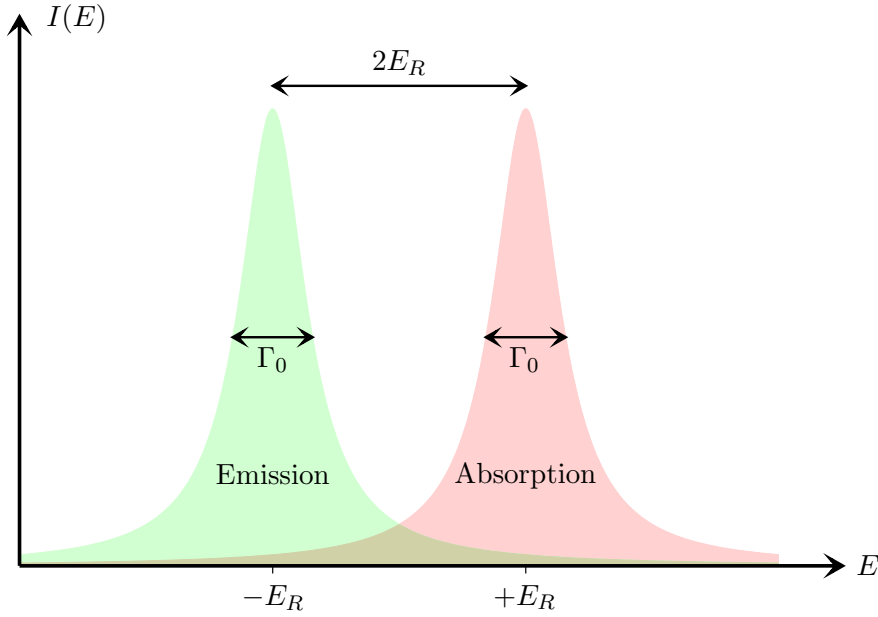


Figure 2.2: Resonant emission and absorption.

2.1.1 Recoil-free fraction and Lamb–Mößbauer factor

In the above section we have seen that the probability for absorption is diminished because of the energy discrepancy due to recoil.

Instead of a single atom, we will now extend our consideration to an atom bound in a lattice. Even though the atom is not rigid in the crystal but has some freedom to vibrate around its equilibrium lattice position, the recoil momentum is taken up by the whole crystal. This is due to the fact that the mean displacement of the atom about its lattice position averages to zero during the time of the nuclear decay. That means, equation (2.4) applies, where M is now the mass of the whole crystal, which shows that the recoil energy can be neglected.

By quantum mechanics we know that the lattice vibrations of a crystal are quantized. Such quantized modes of vibration are called phonons. As a consequence the vibrational energy can only be transferred to the crystal in discrete amounts. Thus, in the case that the atom bound in the crystal emits a γ -ray photon, there are two possible cases which might occur:

1. no phonon is transmitted to the crystal: the recoil energy of an atom bound in a crystal is transferred to the whole crystal, which results in a negligible recoil energy, or
2. the energy of one phonon is transmitted to the crystal: the recoil energy is transferred to the lattice by increasing (or lowering) its lattice vibrations.

Let f be the fraction of events where case (1) occurs, that is where the vibrational

energy of the lattice is unchanged and the energy of the γ -ray photon is not decreased due to recoil but is equal to the energy of the nuclear transition E_0 ($E_\gamma = E_0$). We call f the fraction of zero-phonon transitions. Then $1 - f$ is the fraction of events due to case (2) resulting in a change of the lattice vibrational energy.

In Mößbauer spectroscopy one is interested in a fine energy resolution, which is defined by the measurable linewidth. Case (2) results in a broadening of the line by several orders of magnitude due to thermal vibrations. Therefore the useful information is given by the γ -ray photons due to case (1), photons due to case (2) just contribute to the background.

In other words, the recoil-free fraction f is of prime importance for Mößbauer spectroscopy, even more, resonance emission and absorption is a necessary requirement for observing a Mößbauer spectrum. So far, one can qualitatively say the following about the fraction of zero-phonon transitions f : it gets greater the smaller the γ -ray energy E_γ , the stronger the binding of the atom in the crystal and the lower the temperature.

If one wants to gain an explicit expression for f one has to use a model for the vibrational modes of the crystal. In the Debye model (1912) the density of states is given by

$$\rho(\omega) = \begin{cases} \frac{9N}{\omega_D^3} \omega^2, & \omega \leq \omega_D \\ 0, & \omega > \omega_D. \end{cases} \quad (2.5)$$

The oscillatory frequencies range from zero to a maximum frequency ω_D , the so-called Debye frequency. A characteristic temperature, namely the Debye temperature θ_D is defined through the relation $\hbar\omega_D = k_B\theta_D$. The Debye model leads to the following formula for the recoil-free fraction f :

$$f = \exp \left\{ -\frac{6E_R}{k_B\theta_D} \left[\frac{1}{4} + \left(\frac{T}{\theta_D} \right)^2 \int_0^{\theta_D/T} \frac{x dx}{e^x - 1} \right] \right\}. \quad (2.6)$$

This can also be written in the form $f = \exp(-2W)$, where W is called the Lamb-Mößbauer factor. The way to derive expression (2.6) can be looked up in [Wegener66, Chapter 3] or [Greenwood71, Section 1.4]. The low, respectively high temperature limit is given by

$$f = \begin{cases} \exp \left\{ -\frac{E_R}{k_B\theta_D} \left[\frac{3}{2} + \frac{\pi^2 T^2}{\theta_D^2} \right] \right\}, & T \ll \theta_D, \\ \exp \left\{ -\frac{6E_R T}{k_B\theta_D^2} \right\}, & T \geq \frac{1}{2}\theta_D. \end{cases} \quad (2.7)$$

2.1.2 Natural linewidth

As mentioned in the end of Section 2.1 the energy difference E_0 between excited state E_g and ground state E_0 of an atom is not sharply defined. Rather there exists a spread of the energy ΔE . This is equivalent to there being no exactly defined time for which the atom remains in the excited state before it decays. This uncertainty in time is denoted by Δt .

An excited state has a mean life time τ_0 , which is related to the uncertainty of the γ -ray energies Γ_0 (the decay width) by the Heisenberg uncertainty principle

$$\tau_0 \Gamma_0 = \hbar.$$

We will now deduce the frequency spectrum $I(\omega)$. The energy difference between the ground E_g and excited state E_e is given by

$$E_e - E_g = E_0 = \hbar\omega_0.$$

From quantum mechanics we know that the radiation field of a nuclear decay is exponentially decreasing with time (decay constant $\Gamma_0/2$)

$$\vec{E}(t) \propto \exp(iE_g t/\hbar - i(E_e - i\Gamma_0/2)t/\hbar) = \exp(-i(\omega_0 - i\Gamma_0/2\hbar)t). \quad (2.8)$$

Let us now compute the Fourier transform of \vec{E} , i.e.,

$$F(\omega) \propto \int_0^{+\infty} \vec{E} \exp(i\omega t) dt = \frac{1}{\omega - \omega_0 + i\Gamma_0/2\hbar}. \quad (2.9)$$

This leads to the following frequency spectrum, the so-called Breit–Wigner distribution [Breit36]:

$$I(\omega) = |F(\omega)|^2 \propto \frac{1}{(\omega - \omega_0)^2 + (\Gamma_0/2\hbar)^2}. \quad (2.10)$$

To non-physicists this function is also known as Lorentz- or Cauchy distribution, which has its maximum at ω_0 and mean width Γ_0 (also called natural line width or decay width), see Figure 2.3.

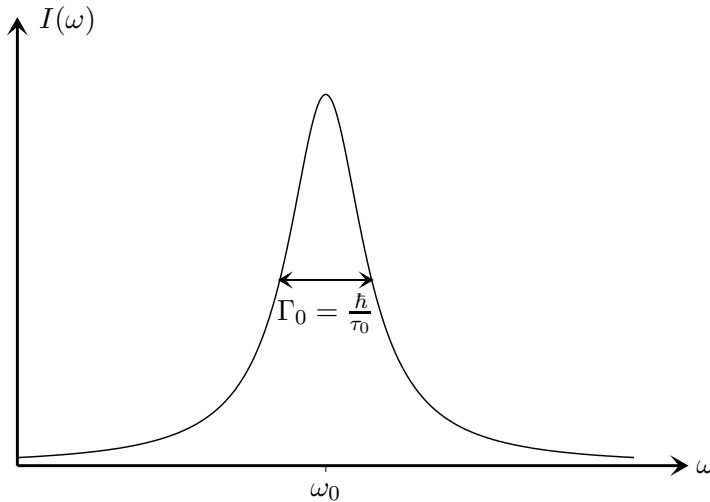


Figure 2.3: Lorentzian distribution of a spectral line.

In the typical case of a ^{57}Fe -nucleus the energy difference of the ground state E_g to the first excited state E_e is given by $E_0 = E_e - E_g = \hbar\omega_0 = 14.4$ keV. The half-life time is $t_{1/2} = \tau_0 \ln(2) = 141$ ns, where τ_0 is the mean life time. Hence, the natural line width amounts to $\Gamma_0 = \hbar/\tau_0 = 4.67$ neV. From (2.4) we obtain for the recoil energy of a free Fe-atom $E_R = 1.95$ meV. Obviously, for a free atom, E_R is 10^6 times larger than Γ_0 . This is the reason why the probability of occurrence of resonance emission and absorption for free atoms is very small.

2.2 Hyperfine interactions

Due to the small natural line width of the 14.4 keV-energy level of the ^{57}Fe -isotope, changes in the position and the shape of the resonance line can be detected with very high resolution. Such changes can be due to hyperfine interactions, i.e. interactions of the electric and magnetic moments of the nucleus with the internal fields at the location of the nucleus. The principal hyperfine interactions that can be observed with Mößbauer spectroscopy are the chemical isomer shift, the electric quadrupole splitting and the magnetic hyperfine structure.

2.2.1 Chemical isomer shift

The main reference for this section was [Wegener66, Chapter 5]. The chemical isomer shift and the electric quadrupole splitting are caused by the electric interaction of the nucleus with its chemical environment. The interaction energy between a nuclear charge with density $\rho(\vec{r})$ and a potential $U(\vec{r})$ is given by

$$E = \int \rho(\vec{r})U(\vec{r})d^3r.$$

Expanding the potential $U(\vec{r})$ into a Taylor series at the origin $\vec{r} = 0$ one can write E in the form

$$E = V(I) + V(Q),$$

where the term $V(I)$ gives the chemical isomer shift and the second term $V(Q)$ the electric quadrupole splitting. Let us introduce a nuclear root mean square radius $\langle r^2 \rangle$ by

$$\int \rho \cdot r^2 d^3r = Ze\langle r^2 \rangle.$$

In the case of a transition from the excited (e) to the ground state (g) the following expression contributes to the energy:

$$V_e(I) - V_g(I) = \frac{2\pi Ze^2 |\psi(0)|^2}{3} (\langle r^2 \rangle_e - \langle r^2 \rangle_g),$$

where $|\psi(0)|^2$ denotes the electron density at the position of the nucleus. In the general case the Mößbauer source (S) and the absorber (A) will not be the same substance. This is why we have to distinguish between $|\psi(0)|_S^2$ and $|\psi(0)|_A^2$. The energy difference

between source and absorber, which is called the chemical isomer shift δ , is then given by

$$\delta = \frac{2\pi Z e^2}{3} (|\psi(0)|_A^2 - |\psi(0)|_S^2) (\langle r^2 \rangle_e - \langle r^2 \rangle_g). \quad (2.11)$$

If we consider the nuclei to be spheres of radius R and having a constant charge distribution one can calculate the root mean square radius

$$\langle r^2 \rangle = \frac{1}{Ze} \int \rho \cdot r^2 d^3r = \frac{3}{5} R^2.$$

If the radii of the excited and the ground state only differ by a small amount, namely $\delta R = R_e - R_g$, one finally obtains for the chemical isomer shift

$$\delta = \frac{4\pi Z e^2 R^2}{5} (|\psi(0)|_A^2 - |\psi(0)|_S^2) \frac{\delta R}{R}. \quad (2.12)$$

2.2.2 Electric quadrupole interactions

The term $V(Q)$ which gives the electric quadrupole splitting can be written as (cf. [Wegener66, Chapter 5])

$$V(Q) = \frac{eQV_{zz}}{4} \frac{3m^2 - j(j+1)}{3j^2 - j(j+1)}, \quad (2.13)$$

where V_{zz} denotes the electric field gradient at the location of the nucleus and eQ the quadrupole moment of the nucleus. j is called the spin quantum number and m the magnetic quantum number. The latter is the component of the nuclear spin in the direction of the magnetic field.

Note that $V(Q)$ vanishes if the nuclear spin j is less than 1, which is due to the fact that the quadrupole moment eQ vanishes in this case (for a detailed proof we refer to [Wegener66, Section 5.B]). This is the reason why in the case of the nucleus being the ^{57}Fe -isotope, where $j_e = 3/2$ and $j_g = 1/2$, only the excited state will show a quadrupole splitting. There exist two lines of the electric hyperfine structure, since $V(Q)$ only depends on the square of the magnetic quantum number m . These two lines belong to the quantum numbers $m_e = \pm 3/2$ and $m_g = \pm 1/2$. One gets the following separation of the two lines

$$\Delta E_Q = V(Q) \left(\frac{3}{2}; \pm \frac{3}{2} \right) - V(Q) \left(\frac{3}{2}; \pm \frac{1}{2} \right) = \frac{eQV_{zz}}{2}. \quad (2.14)$$

In Mößbauer spectroscopy one measures $\Delta V(Q)$ through the Doppler effect $\omega_0 \cdot \Delta v$, such that

$$\Delta V(Q) = \frac{eQV_{zz}}{2} = \omega_0 \cdot \Delta v.$$

This has the consequence that if one knows the splitting of the velocity Δv and the nuclear quadrupole moment Q one can easily determine the electric field gradient V_{zz} .

2.2.3 Magnetic hyperfine interactions

The most important hyperfine interaction in our context is the nuclear Zeeman effect, which occurs if there exists a magnetic field at the location of the nucleus. Let us assume that there is a magnetic field with the flux density H .

The Hamiltonian describing the magnetic dipole hyperfine interaction, i.e. the magnetic interaction between the nucleus with the nuclear magnetic moment $\vec{\mu}$ and the magnetic field \vec{H} , is then given by

$$\mathcal{H} = -\vec{\mu} \cdot \vec{H} = -g\mu_N \vec{I} \cdot \vec{H}. \quad (2.15)$$

Here \vec{I} denotes the nuclear spin, μ_N the nuclear Bohr magneton ($\mu_N = e\hbar/2Mc$) and g the nuclear g -factor ($g = \mu/(I\mu_N)$). The eigenvalues of the Hamiltonian \mathcal{H} are given by

$$E_m = -g\mu_N H m, \quad (2.16)$$

where m is the magnetic quantum number, which can take the $2j + 1$ values $-j, -j + 1, \dots, j - 1, j$. Due to the magnetic field existing at the location of the nucleus the nuclear level of spin j splits up into $2j + 1$ equi-distanced non-degenerate substates. We will distinguish between the excited (e) and the ground state (g) by introducing the following quantities: $\mu_e, j_e, m_e, \mu_g, j_g$ and m_g . The ^{57}Fe -isotope has the spin quantum numbers $j_g = 1/2$ and $j_e = 3/2$. Therefore, the excited state (e) splits into four and the ground state (g) into two substates. The Mößbauer transition from the excited to the ground state can take place between two nuclear energy levels if the change in the magnetic quantum number is 0 or ± 1 , i.e. $|m_e - m_g| \leq 1$. In the case of ^{57}Fe there exist six allowed transitions.

If there is no magnetic field H acting at the location of the nucleus the energy of the γ -ray photon $E_\gamma = \hbar\omega_0 = E_e - E_g$ is independent of the magnetic quantum numbers. Then there appears only one line in the Mößbauer spectrum. If the magnetic field $H \neq 0$ is strong enough such that the energy levels split up and the distance between the substates, which is given by $H\mu_e/j_e$ and $H\mu_g/j_g$, is larger than the natural line width, one can observe six lines in the Mößbauer spectrum, the so-called Mößbauer sextet. Each of these lines determines a Lorentz distribution with the mean width $\Gamma_0 = \hbar/\tau_0$. The way how the overall intensity is shared among these six lines depends on the angle between the magnetic field and the direction of propagation of the γ -ray photon. This will be the main topic of Section 2.2.4.

In Mößbauer spectroscopy one typically uses a non-magnetic source, such that the resulting spectrum does not get unnecessarily complicated. That means, the spectrum is easier to evaluate and nevertheless provides the whole necessary information. For this purpose one uses a source material where there does not exist a magnetic field at the location of the nucleus, such that the splitting due to magnetic hyperfine interactions is left to the absorber.

2.2.4 Relative intensities of absorption lines

As mentioned above, the relative intensities of the hyperfine lines depend on the orientation in the single-crystal absorber. More precisely, the intensities are determined by two terms, one being angular dependent and the other angular independent. The intensity of the respective components in a certain direction is given by

$$\text{Intensity} \propto C(m_g, m_e)^2 \Theta(J, m). \quad (2.17)$$

Here the factors $C(m_g, m_e)$ are called the Clebsch–Gordan coefficients, which depend on the magnetic quantum numbers m_g and m_e of the ground and excited state, respectively. These coefficients determine the angular independent terms. In the case of the Mößbauer ^{57}Fe -isotope the decay is given by a dipole transition. Therefore, $m = m_g - m_e$ can only take the values 0 or ± 1 . That is why there are six allowed transitions (instead of eight, since two of them have zero probability). The values of the Clebsch–Gordan coefficients $C(m_g, m_e)$ for a dipole $\frac{3}{2}, \frac{1}{2}$ transition can be looked up in Table 2.1.

m_1	m_g	C	C^2	Θ	$C^2\Theta$
$+\frac{3}{2}$	$+\frac{1}{2}$	1	3	$1 + \cos^2 \theta$	$3(1 + \cos^2 \theta)$
$+\frac{1}{2}$	$+\frac{1}{2}$	$\sqrt{\frac{2}{3}}$	2	$2 \sin^2 \theta$	$4 \sin^2 \theta$
$-\frac{1}{2}$	$+\frac{1}{2}$	$\sqrt{\frac{1}{3}}$	1	$1 + \cos^2 \theta$	$1 + \cos^2 \theta$
$-\frac{3}{2}$	$+\frac{1}{2}$	0	0	0	0
$+\frac{3}{2}$	$-\frac{1}{2}$	0	0	0	0
$+\frac{1}{2}$	$-\frac{1}{2}$	$\sqrt{\frac{1}{3}}$	1	$1 + \cos^2 \theta$	$1 + \cos^2 \theta$
$-\frac{1}{2}$	$-\frac{1}{2}$	$\sqrt{\frac{2}{3}}$	2	$2 \sin^2 \theta$	$4 \sin^2 \theta$
$-\frac{3}{2}$	$-\frac{1}{2}$	1	3	$1 + \cos^2 \theta$	$3(1 + \cos^2 \theta)$

Table 2.1: Relative probabilities for a dipole $\frac{3}{2}, \frac{1}{2}$ transition.

Table 2.1 shows that there are six finite values of the Clebsch–Gordan coefficients $C(m_g, m_e)$. The theoretical intensity ratios for a ^{57}Fe -Mößbauer spectrum are seen to be $3 : 2 : 1 : 1 : 2 : 3$.

The angular dependent terms, given by the functions $\Theta(J, m)$, describe the radiation probability in a direction enclosing an angle θ to the principal axis of the magnetic field. Here J denotes the sum $J = I_g + I_e$, where I_g and I_e is the nuclear spin of the ground and excited state, respectively. The final relative intensities $C^2\Theta$ of the hyperfine lines of a ^{57}Fe -Mößbauer spectrum are given in Table 2.1. The ratios of these intensities are seen to be $3 : x : 1 : 1 : x : 3$, where $x = 4 \sin^2 \theta / (1 + \cos^2 \theta)$. Thus, the relative intensities for the γ -ray direction parallel ($\theta = 0^\circ$) and perpendicular ($\theta = 90^\circ$) to the principal axis of the magnetic field in the single-crystal absorber are $3 : 0 : 1 : 1 : 0 : 3$ and $3 : 4 : 1 : 1 : 4 : 3$, respectively. That means that the value x varies from 0 to 4 as the angle changes from 0° to 90° .

2 Mößbauer spectroscopy

Above considerations play a major role in Mößbauer spectroscopy, since from the relative intensities of the hyperfine lines in the Mößbauer spectrum one can draw conclusions about the orientation of magnetization in the absorber.

Even more information can be obtained by using synchrotron radiation with its well-defined linear polarization.

3 Phase transformations

In this chapter, which is based on [Pfeiler07], we will study the theory of nucleation and growth transformations as well as the kinetics of such transformations.

3.1 Theory of nucleation

Let us consider a α - β -phase transition in a specific material. Suppose this material, which originally consists of a homogeneous α -phase, is exposed to temperatures where the β -phase is stable. Then there will occur nuclei of the β -phase after some time. These nuclei will grow such that after a specific time no areas of α -phase are present any more in the material. At this point the α - β -phase transition is complete.

There is a wide range of mechanisms for such phase transitions. One way to classify these mechanisms is to distinguish between homogeneous and heterogeneous nucleation. The former refers to nuclei that are formed randomly distributed in the material, i.e. there exists no preferred location of occurrence. The latter refers to the formation of nuclei at specific locations of the material. Heterogeneous nucleation usually appears at defects in the crystal, such as grain boundaries, dislocation lines, etc.

3.1.1 Critical nucleus

The probability \mathcal{P} that a β -nucleus is formed in a unit volume of the α -parent phase is given by

$$\mathcal{P}(T) \propto \exp\left(-\frac{W}{k_B T}\right). \quad (3.1)$$

Here W denotes the work of formation and is given by

$$W = V\Delta G + A\sigma, \quad (3.2)$$

where A is the surface of the nucleus, σ the surface energy, V the volume of the β -phase and ΔG the Gibb's free energy per unit volume, which is released when forming the new β -phase from the parent α -phase. Let us suppose that the nucleus of the β -phase has the shape of a sphere of radius R , since this form optimizes the surface-to-volume ratio. Moreover, we will assume that the surface energy σ is isotropic. Then equation (3.2) reads

$$W(R) = \frac{4}{3}\pi R^3 \Delta G + 4\pi R^2 \sigma. \quad (3.3)$$

The nucleus is stable if $\Delta G < 0$ and the radius R of the nucleus is large enough. Then the effort contributing to the surface energy is compensated for by the energy gained

3 Phase transformations

from the growing volume. This means that the negative term in equation (3.3) depends on R^3 whereas the positive term varies with R^2 . As can be seen from Figure 3.1 this has the consequence that the formation energy $W(R)$ has a maximum at a certain radius R^* . For all $R < R^*$ the formation energy $W(R)$ increases whereas for $R > R^*$

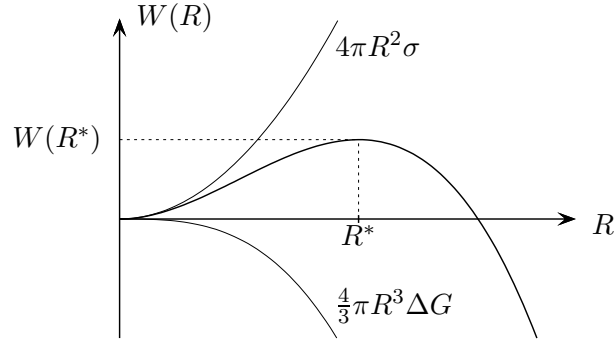


Figure 3.1: Formation energy $W(R)$ depending on the radius of the nucleus R .

it is a decreasing function. That is why a nucleus of radius $R < R^*$ will not grow, rather it will dissociate. However, a nucleus with $R > R^*$ will grow very likely by atom attachment.

We call the radius R^* , where the function $W(R)$ has its maximum, critical radius, and similarly the nucleus with radius R^* the critical nucleus. We can explicitly determine the critical radius R^* by differentiation of the formation energy:

$$\begin{aligned} \left. \frac{dW(R)}{dR} \right|_{R=R^*} &= 4\pi(R^{*2}\Delta G + 2R^*\sigma) = 0 \\ R^* &= -\frac{2\sigma}{\Delta G}. \end{aligned} \quad (3.4)$$

The critical work of formation $W^* = W(R^*)$ is then given by

$$W^* = \frac{16\pi\sigma^3}{3\Delta G^2}. \quad (3.5)$$

3.1.2 Heterogeneous nucleation

In reality, homogeneous nucleation only appears under ideal circumstances. Usually, nucleation is of the heterogeneous type, where nuclei are built at dislocations and grain boundaries.

In the case of homogeneous nucleation we have assumed that the nuclei have the form of a sphere (cf. Section 3.1.1). However, in the case of heterogeneous nucleation the situation is different, since the nuclei occur not randomly distributed in the bulk material, rather they are formed at defects. Let us consider the nucleation at a grain boundary, then the elimination of the grain boundary area causes the shape of the

3.1 Theory of nucleation

nucleus to be a double spherical cap with contact angle ϕ instead of a sphere. The surface area is given by

$$A = 4\pi(1 - \cos \phi)R^2$$

and the volume by

$$V = \frac{2\pi}{3}(2 - 3\cos \phi + \cos^3 \phi)R^3.$$

Thus, the formation energy (3.2) now reads

$$W(R, \phi) = \frac{2\pi}{3}(2 - 3\cos \phi + \cos^3 \phi)R^3 \Delta G + 4\pi(1 - \cos \phi)R^2 \sigma - \pi R^2 \sin^2 \phi \sigma_{\text{gb}}, \quad (3.6)$$

where the last term contributes to the energy saving that occurs if a part of a grain boundary is eliminated. σ_{gb} denotes the grain boundary energy. The critical radius is the same as in the case of homogeneous nucleation, i.e.

$$R^* = -\frac{2\sigma}{\Delta G}. \quad (3.7)$$

Plugging this expression into (3.6) we get

$$W(R^*, \phi) = \frac{16\pi}{3} \frac{\sigma^3}{\Delta G^2} (1 - \cos^3 \phi) - 4\pi \sin^2 \phi \frac{\sigma^2}{\Delta G^2} \sigma_{\text{gb}}. \quad (3.8)$$

To find the critical angle ϕ^* one has to differentiate this expression with respect to ϕ and set it equal zero

$$\begin{aligned} \left. \frac{dW(R^*, \phi)}{d\phi} \right|_{\phi=\phi^*} &= 8\pi \frac{\sigma^2}{\Delta G^2} \cos \phi^* \sin \phi^* (2\sigma \cos \phi^* - \sigma_{\text{gb}}) = 0 \\ 2\sigma \cos \phi^* &= \sigma_{\text{gb}}. \end{aligned} \quad (3.9)$$

Then we finally obtain the critical formation energy

$$\begin{aligned} W^* = W(R^*, \phi^*) &= \frac{16\pi}{3} \frac{\sigma^3}{\Delta G^2} \left(1 - \left(\frac{3}{2} \cos \phi^* - \frac{1}{2} \cos^3 \phi^* \right) \right) \\ &= W_{\text{hom}}^* \frac{2 - 3\cos \phi^* + \cos^3 \phi^*}{2}, \end{aligned} \quad (3.10)$$

or equivalently

$$W^* = W(R^*, \phi^*) = \frac{16\pi}{3} \frac{\sigma^3}{\Delta G^2} \left(1 - \frac{1}{2} \left(\frac{3\sigma_{\text{gb}}}{2\sigma} - \frac{\sigma_{\text{gb}}^3}{8\sigma^3} \right) \right) = W_{\text{hom}}^* \frac{16\sigma^3 - 12\sigma^2 \sigma_{\text{gb}} + \sigma_{\text{gb}}^3}{16\sigma^3},$$

where W_{hom}^* is defined in (3.5). Since the contact angle ϕ^* can range from 0° to 90° we have $0 \leq (2 - 3\cos \phi^* + \cos^3 \phi^*)/2 \leq 1$. Hence, from equation (3.10) it can be seen that the energy of formation of a nucleus at a grain boundary is always less than the one of a homogeneous nucleus.

3.2 Kinetics of phase transformations

3.2.1 The Kolmogorov-Johnson-Mehl-Avrami equation

In this section we consider the temporal evolution of an α - β -phase transition. The theory of the time dependence of the volume fraction of the transformed β -phase in an α -matrix phase was developed by Kolmogorov ([Kolmogorov37]), Johnson and Mehl ([Johnson39]), and Avrami ([Avrami39], [Avrami40], [Avrami41]). They supposed the nuclei to be spherical and the radius $r(t)$ of a nucleus to be a convex function of time t . Under these assumptions the transformed fraction f as a function of time t is given by

$$f(t) = 1 - \exp\left(-\frac{4\pi}{3} \int_0^t I(\tau)(r(t-\tau))^3 d\tau\right), \quad (3.11)$$

where $I(\tau)$ denotes the nucleation rate per unit volume and $r(t-\tau)$ the radius of the β -nuclei.

Now we will describe how to deduce equation (3.11). If all β -particles could grow independent of each other (that is without impingement), they would occupy the so-called extended volume $V_{\beta,e}$ of the transformed phase. If we make the assumption of spherical β -particles and a homogeneous nucleation rate per unit volume I the extended volume $V_{\beta,e}$ can be written as

$$V_{\beta,e}(t) = \frac{4\pi}{3} V \int_0^t I(\tau)v(\tau,t)d\tau, \quad (3.12)$$

where particles which nucleate at a time τ have a volume $v(\tau,t) = (r(t-\tau))^3$, i.e., a radius $r(t-\tau)$ at a later time t . Here V denotes the total volume of the system. Let us denote by V_β the fraction of the volume V that has already been transformed, then the volume fraction which remains untransformed is given by $(1 - V_\beta/V)$. The increase of the artificial volume $V_{\beta,e}$ only results in an increase of the actual volume V_β if the would-be transformation occurs in a not yet transformed volume of the material.

Let us make the assumption that nucleation and growth of the β -phase happens homogeneous in the parent α -phase. Then one deduces that the probability that a specific point in the material has not yet been transformed into the β -phase is given by

$$dV_\beta = \left(1 - \frac{V_\beta}{V}\right) dV_{\beta,e} \quad (3.13)$$

and after integration

$$\frac{V_\beta}{V} = 1 - \exp\left(-\frac{V_{\beta,e}}{V}\right). \quad (3.14)$$

Inserting (3.12) then yields

$$f(t) = \frac{V_\beta}{V} = 1 - \exp\left(-\frac{4\pi}{3} \int_0^t I(\tau)r^3(t-\tau)d\tau\right), \quad (3.15)$$

which is seen to be of the form (3.11).

Equation (3.11) is often written in the form

$$f(t) = 1 - \exp\left(-\left(t/\tau\right)^n\right), \quad (3.16)$$

the so-called Johnson-Mehl-Avrami-Kolmogorov (JMAK) equation. For small t the growth of the transformed phase follows a power law. After a particular time the volumes of the β -particles begin to overlap and thus the transformed fraction f asymptotically approaches the equilibrium state. Here n denotes the Avrami-exponent which is a characteristic constant of the type of nucleation process. It usually varies between 1 and 4 and can also take non-integer values. The variable τ denotes a time constant which strongly depends on the temperature, i.e., the degree of under-cooling. We will now consider two important special cases:

- (i) First, assume that the nucleation rate density $I(\tau)$ (number of nuclei built per time and volume) vanishes ($I(\tau) \equiv 0$), that is a specific number density N/V of β -nuclei exist at time $t = 0$ but none are generated at any later time. Suppose the nuclei grow with the rate $r(t) = vt$ for some constant v . Equation (3.11) then becomes

$$f(t) = \frac{V_\beta(t)}{V} = 1 - \exp\left(-\frac{4\pi}{3}v^3\frac{N}{V}t^3\right). \quad (3.17)$$

Equation (3.17) is of the form (3.16) with $n = 3$ and $\tau^{-3} = \frac{4\pi}{3}v^3\frac{N}{V}$.

- (ii) Second, we make the assumption of a constant nucleation rate density $I(\tau) \equiv I$ and again a growth rate $r(t) = vt$ of the nuclei. Then integration of equation (3.11) yields

$$f(t) = \frac{V_\beta(t)}{V} = 1 - \exp\left(-\frac{\pi}{3}v^3It^4\right), \quad (3.18)$$

which is of the form (3.16) with $n = 4$ and $\tau^{-4} = \frac{\pi}{3}v^3I$.

Physically plausible mechanisms give Avrami exponents between 1 and 4. Fitting (3.16) to experimental data can therefore indicate the mechanism of the phase transition.

4 Experimental details

This chapter consists of two parts: the first one gives a detailed description of the equipment which is necessary for Mößbauer spectroscopy. This part contains remarks on the Mößbauer source, the electronics of the Mößbauer spectrometer and the calibration.

The second part of this chapter addresses the issue of the production of the samples and their treatment during experimentation.

4.1 The Mößbauer spectroscopy equipment

The Mößbauer spectroscopy setup consists of a single line-source, the absorbing sample, the detector and the electronics for measuring a Mößbauer spectrum.

4.1.1 Source

As mentioned in Section 2.2.3, in Mößbauer spectroscopy it is principally desirable to use a single line-source, so that the splitting due to hyperfine interactions is left to the absorbing sample. The source we were making use of was a Rh-foil in which ^{57}Co was incorporated by electrodeposition and annealing.

The nuclear processes of a ^{57}Co source are shown in Figure 4.1. ^{57}Co decays by electron capture to ^{57}Fe , which is left in an excited state of 137 keV due to the released energy of the nuclear decay. Then there are two possibilities that might occur: the first one is the transition from this excited state directly to the ground state (91%) or the nucleus decays from the excited state of 137 keV to the one of the energy 14.4 keV and subsequently after a half life time of 98 ns to the ground state. The latter process is the one important to Mößbauer spectroscopy.

4.1.2 Electronics of the Mößbauer spectrometer

The scheme of a typical Mößbauer spectrometer is shown in Figure 4.2.

In Mößbauer spectroscopy one wants to modulate the energies of the γ -photons, which are emitted by the source due to transition of the 14.4 keV state to the ground state. Experimentally this is realized in the following way: the source is fixed at the Mößbauer driving unit (MDU). For the movement of the unit one uses a loudspeaker. Thus, due to the Doppler effect, also the energies of the emitted γ -photons are varied. These γ -rays of different energy are then absorbed by or pass through the sample, depending on the possibility to create an excited state in the sample by the proper energy of a γ -photon.

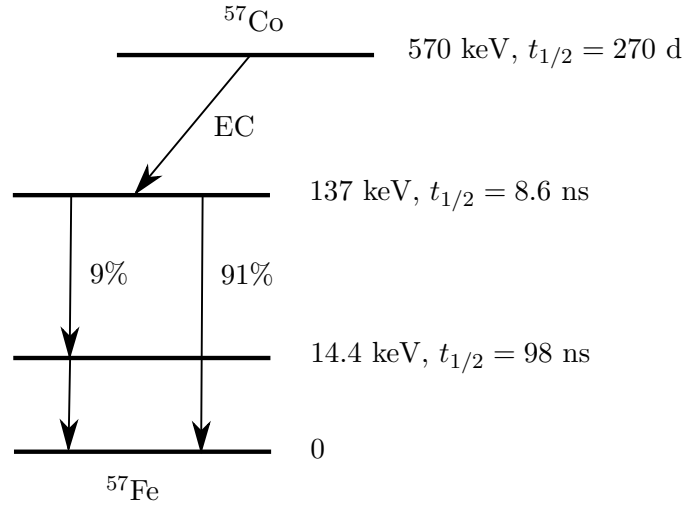


Figure 4.1: Nuclear processes of a ^{57}Co source.

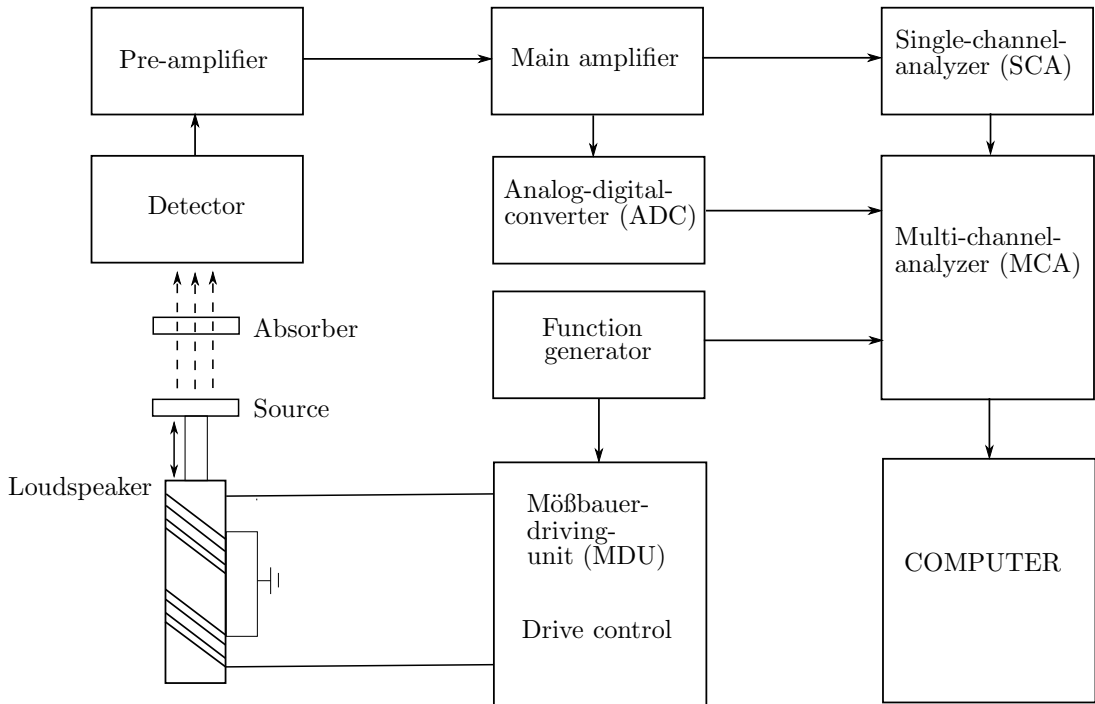


Figure 4.2: Scheme of the Mößbauer spectrometer.

The γ -rays that pass through the absorber are counted by a γ -detector positioned behind the sample. This detector is a proportional counter filled with a Krypton-Methane-mixture, i.e. the detector generates voltage pulses that are proportional to

4.2 Preparation and treatment of the samples

the energy of the detected γ -rays. That is, only the γ -rays that are transmitted are detected and we therefore get a spectrum of transmission.

The first element in the chain of signal processing is the pre-amplifier, which gets the pulses from the detector. Then the signal passes the main amplifier and reaches the single-channel-analyzer (SCA). This element completes the task of selecting pulses that lie between two adjustable pulse heights. This offers the opportunity to fade out pulses due to fluorescence effects and cosmic radiation. If the pulse lies in the selected energy window the multi-channel-analyzer (MCA) receives a pulse signal. The MCA counts all pulses coming from the SCA in a specific channel until there happens a shift to the next channel. Such a shift can be controlled by the function generator. During a period all channels are switched through with regular time intervals. After one period the MCA switches again to the first channel. The analog-digital-converter (ADC) is used for calibration of the energy window.

The function generator also has the task of predefining the velocity profile. The drive control does the job of comparing the actual with the desired value of the inductor of the loudspeaker and finally to correct by negative feedback. This allows a precision of 10^{-4} of the velocity of the Mößbauer drive following the reference signal coming from the function generator.

In this manner a Mößbauer spectrum, i.e. the number of counts per channel vs. number of the channel, is recorded.

For the visualization and the evaluation of this Mößbauer spectrum one uses a computer. The first thing one has to do is to calibrate, that is to correlate the channels with the right velocities, i.e. energies (cf. Section 4.1.3). During a period all velocities appear twice, such that the Mößbauer spectrum is recorded twice too. Thus the next thing one has to do is to fold the obtained transmission spectrum to get a single Mößbauer spectrum. Finally one can fit the spectrum. All steps, i.e. calibrating, folding, and fitting were done with the program RECOIL (cf. Section 6.1).

4.1.3 Calibration

To associate the channels of the MCA with the appropriate velocities one has to calibrate the Mößbauer spectrometer. For this purpose one measures the transmission spectrum of a magnetic Fe-foil, which is $25\ \mu\text{m}$ thick and has a purity of 99.99 %. Since this foil is magnetic the transmission spectrum consists of six lines (cf. Section 2.2.3). The positions of these lines are well-known. Therefore, one can easily correlate the channels with the right velocity- resp. energy-areas.

4.2 Preparation and treatment of the samples

In this section we will shortly describe how the samples of the alloy Fe-Cr were prepared and treated during experimentation.

4.2.1 Preparation of the samples

The samples of $\text{Fe}_{53.8}\text{Cr}_{46.2}$ resp. $\text{Fe}_{51}\text{Cr}_{49}$ were prepared by melting appropriate amounts of Fe (99.95 % purity) and Cr (99.5 % purity) in a vacuum induction furnace. Subsequently, the resulting ingots were cut into cubes of the dimensions $(5 \text{ mm})^3$. These cubes were then homogenized by vacuum annealing for 24 h at 1200°C and finally water-quenched.

The exact chemical composition of the samples were determined by electron probe microanalysis. The concentrations of Fe and Cr were evaluated as an average over five values measured at various places of the sample.

The samples, consisting of the α -phase, were then rolled into sheets of the thickness $10 \mu\text{m}$. Afterwards, these foils were cut into pieces of $7 \text{ mm} \times 7 \text{ mm}$, which were finally transformed from the α into the σ -phase by an isothermal vacuum anneal for 24 h at 700°C .

Then the samples were ready for further treatment.

4.2.2 Treatment of the samples

As our aim was to study the kinetics of the transformation from the σ - into the α -phase in the system Fe-Cr the experimental procedure was the following: the samples, which consisted of the σ -phase after the preparation described above, were alternately vacuum annealed at a certain temperature (at which the α -phase is stable) and ex-situ measured by Mößbauer spectroscopy. In this way one obtained a sequence of Mößbauer spectra (corresponding to the annealing times) for every sample, i.e. for various temperatures.

For the annealing process a self-built furnace was used. This furnace consists of two quartz tubes of different length. Around the shorter tube a wire is wrapped round like a coil. The wire has a very high resistivity such that temperatures up to 1000°C are possible. This quartz tube is put into the other longer tube, which has an accordingly larger diameter. The furnace is insulated by two alternating layers of appropriate materials, namely Al_2O_3 -paper and Al-foil. Moreover, a thermocouple is positioned appropriately in order to control the temperature in the furnace.

Before one sample was pushed into the furnace, the long quartz tube was evacuated by a vacuum pump, which was attached to the end of the tube. Finally, after a vacuum of about 10^{-4} mbar was achieved, the sample was pushed into the preheated furnace for a specific time and subsequently taken out. It was left in vacuum for a few minutes to cool. After that the attachment for the vacuum pump was carefully removed, such that the sample could then be taken out ready to start the Mößbauer measurements.

5 The system iron-chromium

Our investigations of the kinetics of the phase transition between complex phases is not only interesting from the view point of solid state physics, but also for technological reasons.

As Fe-Cr is the base alloy of stainless steels, it is of particular importance to several branches of industry. Recently, the system Fe-Cr has become of growing interest for the technological development of prospective fusion reactors.

The wide application of high-chromium ferritic steels is in particular due to their high-temperature corrosion resistance and resistance to radiation damage. Steels of that kind consist to 90 – 95% of the elements Fe and Cr. Thus, studying the properties and behavior of Fe-Cr under extreme conditions, like high temperatures and high irradiation levels, is the key to draw conclusions about the behavior of these steels subject to these conditions.

To summarize, the investigation of Fe-Cr is of prime importance to all those branches of industry where stainless steel components are used, exposed to elevated temperatures or radiation, such as boilers, heat exchangers, pipes, gas turbines, and components of future fusion and new fission reactors.

If we take a look at the phase diagram of Fe-Cr (see Figure 5.1) we can make the following observations: the α -phase is the high temperature phase, the σ -phase is stable at temperatures less than 821°C and if the chromium content lies between 43 – 49 at.% (cf. [Cook43]). The phase diagram Figure 5.1 implies that the σ -phase is not stable for temperatures less than 475°C. Contradicting that, in [Predel94] the σ -phase is claimed to exist down to room temperature. The author of [Predel94] bases himself on a work done by Kuwano [Kuwano85b] who states that there are no experimental findings for an instability of the σ -phase below 577°C. Thus the lower limit of the temperature range where the σ -phase is stable can be considered a controversial issue in literature. However, this will be of no relevance for our investigations on the σ -to- α -phase transition discussed in this thesis.

On the iron rich side there exists the fcc γ -phase, which is formed at temperatures above 830°C and Cr concentrations less than 12%. Anyway, the γ -phase is not relevant for our purposes.

There are two main phenomena which are of industrial interest that can occur:

1. the precipitation of the σ -phase from the α -matrix phase or
2. the α/α' -phase decomposition, that is a phase decomposition into a Fe-rich α -phase and a Cr-rich α' -phase.

Both are unwanted phenomena in industry for the following reasons:

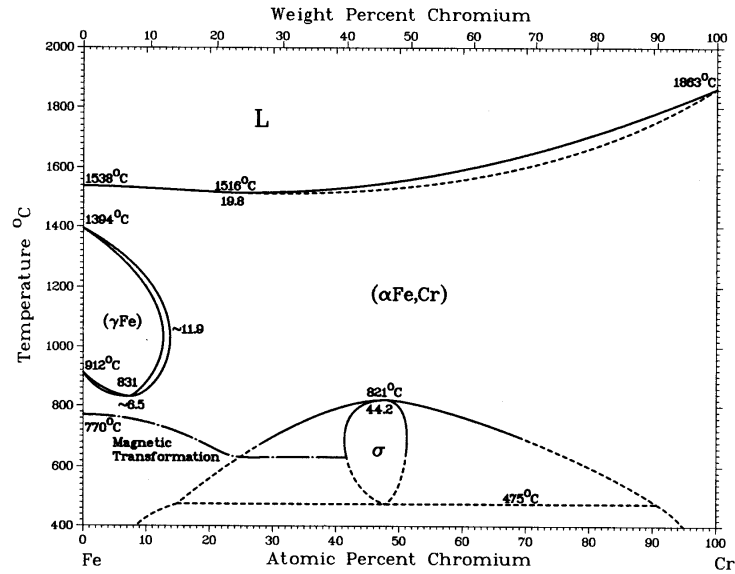


Figure 5.1: The phase diagram of the system Fe-Cr [Massalski90].

1. the σ -phase is characterized by its brittleness. Therefore the precipitation of this phase in stainless steels is very critical, since it deteriorates the properties of the latter: the ductility and corrosion resistance decreases whereas the brittleness increases.
2. the α/α' -phase decomposition results in the unwanted 475°C-embrittlement of the material. This phenomena has been investigated by means of Mößbauer spectroscopy, cf. [Cieślak00b], [Cieślak98], and [Dubiel99].

In the thesis at hand we want to study the σ -to- α phase transformation in Fe-Cr. For this reason we now want to take a detailed look at the two phases involved in this phase transition:

5.1 The σ -phase

The sigma phase appears in many binary and ternary alloy systems, such as Fe-Cr, Fe-V, or Fe-Mo, to name just a few. It was first discovered in the ternary system Fe-Cr-Ni in 1923 [Bain23].

A very important contribution to the study of the σ -phase was made by Bergman and Shoemaker in 1954 [Bergman54]. They were the first ones that determined the crystallographic structure of the σ -phase in Fe-Cr and Fe-Mo alloys. They managed to do so by powder and single-crystal X-ray diffraction. The crystal structure was established as tetragonal ($a_0 = b_0 = 8.799 \text{ \AA}$, $c_0 = 4.546 \text{ \AA}$), belonging to the space group type $D_{4h}^{14} - P4_2/mnm$. The unit cell consists of 30 atoms, these are distributed

over five inequivalent sites, specifically 2 of type A, 4 of type B, and 8 of type C, D, and E, respectively (see Figure 5.2).

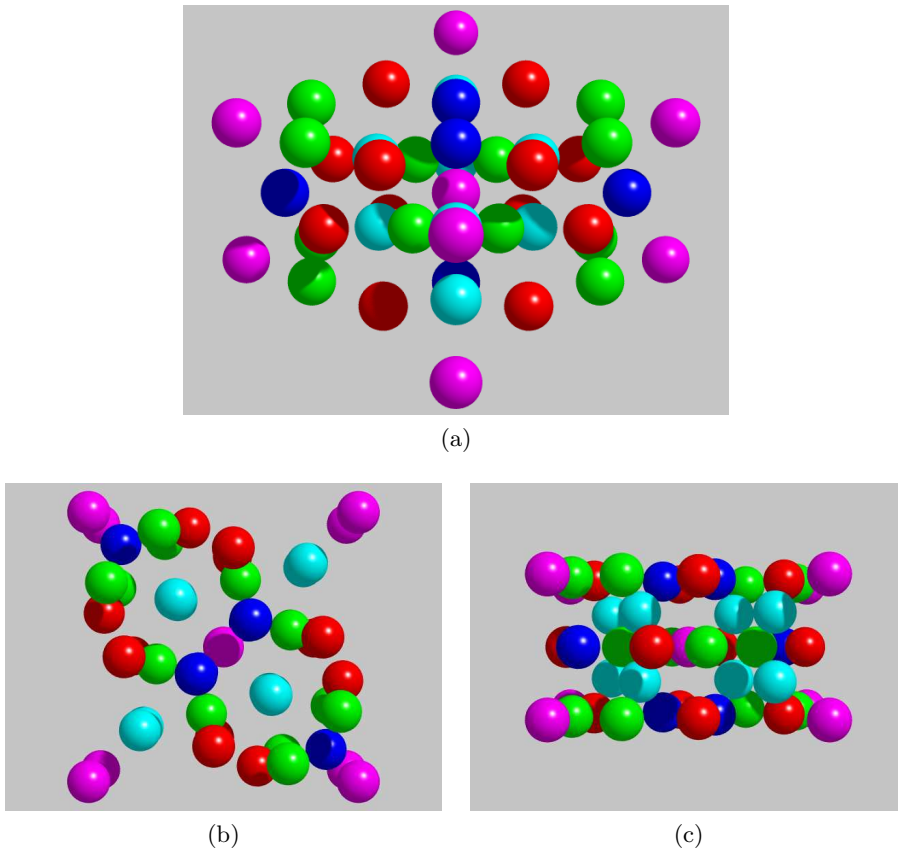


Figure 5.2: The atomic arrangement in the σ -phase unit cell. The five inequivalent sites have different colors: site A (magenta), site B (dark-blue), site C (red), site D (green), and site E (light-blue). The directions of the views are (a) the $[\sqrt{3/2}, \sqrt{3/2}, 1]$ direction, (b) the $[001]$ direction, and (c) the $[010]$ direction.

The structure of the σ -phase turned out to be very interesting. By distorting a hexagonal close-packed (hcp) net a little bit it can be fitted into a tetragonal cell. From this hcp net a few atoms are displaced in such a way that they are positioned between the two closed-packed layers of the hcp net. This leads to an improved overall packing: the atoms positioned intermediate between the layers prevent those to slip. This fact can be considered as one of the key arguments for the brittleness of the σ -phase.

Concerning the Fe and Cr atom distributions over these five sites there were made experimental investigations by H.L. Yakel [Yakel83] and by J. Cieřlak et al. [Cieřlak08a]. In both cases it turned out that there are sites with preferred Fe- or Cr-occupation, but

no site is occupied exclusively by one species. In the experimental work of H.L. Yakel the site occupancy was studied with $\text{MoK}\alpha$ Bragg-diffraction methods, whereas the authors of [Cieślak08a] obtained the site-occupation parameters from neutron diffraction measurements. These two investigations of the site-occupancy in the σ -phase seem to be in good agreement.

In the study of [Cieślak08a] samples of the compositions $\text{Fe}_x\text{Cr}_{1-x}$ with $x = 50.5, 50.9, 52.0, 52.3, 53.8,$ and 54.7 , which were annealed at 973 K for 25 days, were measured. The results of the experiments can be seen in Figure 5.3.

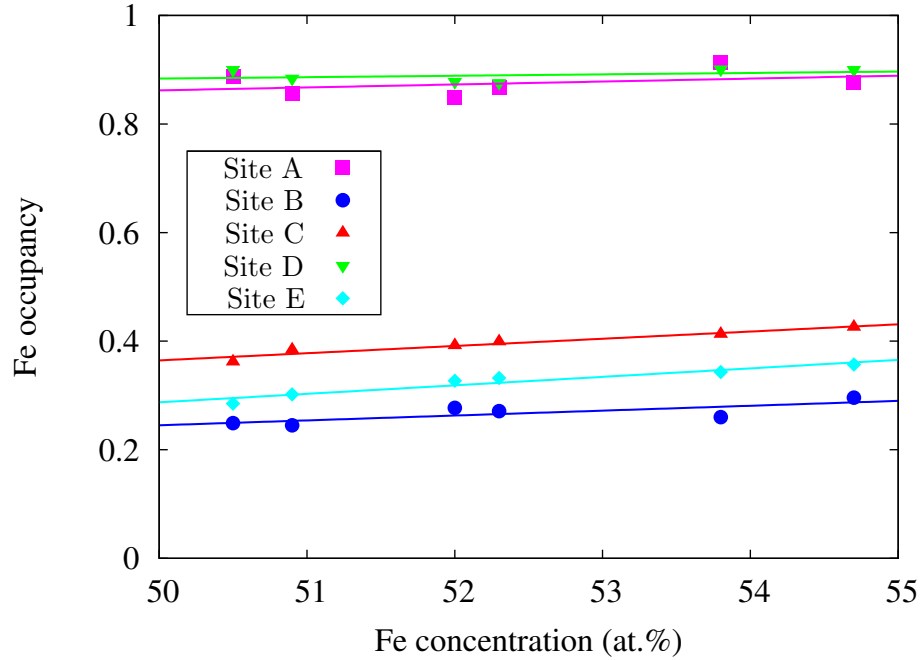


Figure 5.3: The relative site occupation in Fe-Cr σ -phases measured with neutron diffraction methods [Cieślak08a]. The lines are linear fits to the data.

Obviously, there is a strong preference of Fe to occupy the sites A and D. The sites B, C, and E are occupied by both Fe and Cr atoms, where the Cr content is a little bit higher than the Fe one in all of these three sites. Moreover, as the Fe concentration in the sample gets higher an increase of the relative Fe occupancy of the sites can be observed, which is not surprising.

There have also been made computer simulations concerning the site-occupation in the σ -phase by M. Sluiter, K. Esfarjani, and Y. Kawazoe [Sluiter95]. Unfortunately, the results are not in agreement with the experimental data presented in [Yakel83] and [Cieślak08a].

The compositions which were studied in the context of this thesis were $\text{Fe}_{51}\text{Cr}_{49}$ and $\text{Fe}_{53.8}\text{Cr}_{46.2}$. The corresponding Fe occupancies of the five lattice sites, according to

[Cieślak08a], can also be looked up in Figure 5.3.

Table 5.1 indicates the numbers of nearest neighbor (NN) atoms of the five lattice sites, respectively. The values are taken from [Cieślak08b], there also the distances between NN atoms for the five sites of the σ -phase can be looked up.

Site	number of NN atoms					Total
	A	B	C	D	E	
A	-	4	-	4	4	12
B	2	1	2	4	6	15
C	-	1	5	4	4	14
D	1	2	4	1	4	12
E	1	3	4	4	2	14

Table 5.1: Numbers of nearest neighbor (NN) atoms for the five sites in the σ -phase [Cieślak08b].

5.2 The α -phase

The α -phase in the compound Fe-Cr constitutes the high-temperature phase. It has a bcc-structure (see Figure 5.4). The Fe and Cr atoms are distributed randomly over the bcc-lattice sites.

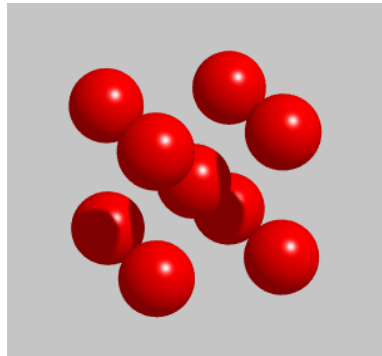


Figure 5.4: The atomic arrangement in the α -phase cubic unit cell.

The short-range-order (SRO) in the α -Fe-Cr phase was investigated theoretically in the pioneering work of M. Hennion [Hennion83] and later also studied experimentally by I. Mirebeau, M. Hennion, and G. Parette [Mirebeau84].

To identify the SRO in a specific A-B alloy one makes use of the Warren-Cowley parameter, often also denoted as SRO parameter. This parameter is a useful tool to compute the pair-probabilities in the alloy. If the SRO parameter is positive a tendency towards building clusters of A resp. B atoms can be observed (repulsive

SRO). A negative SRO parameter corresponds to an ordering tendency (attractive SRO). The exact definition of the SRO parameter can be looked up in [Lavrentiev07a] or [Bonny09].

The authors of [Mirebeau84] made the observation that the SRO parameter in the α -phase is a function of Cr concentration. Even more, the parameter changes its sign if the Cr concentration c_{Cr} in the Fe-Cr compound is near 10 at.% at 703 K. As the SRO parameter is negative for $c_{\text{Cr}} < 10$ at.% the atoms in the alloy tend to distribute themselves such that an ordered compound is built. Whereas, for alloys with $c_{\text{Cr}} > 10$ at.%, where the SRO parameter is positive, there can be observed short-range clustering, that is there appear Fe and Cr clusters.

This result was confirmed recently (cf. [Lavrentiev07a] and [Lavrentiev07b]) by Monte Carlo simulations of an Fe-Cr alloy based on the cluster expansion approximation. Nevertheless, the actual Cr concentration where the sign of the SRO parameter changes turned out to depend on the temperature. The change of sign of the SRO parameter is seen to be near 10 at.% Cr at a temperature $T = 800$ K. Although for higher temperatures, such as $T = 1400$ K or $T = 1600$ K, the change of sign shifts towards lower Cr concentrations, the effect of temperature seems negligible. The SRO parameter is positive for higher Cr concentrations and reaches its maximal value at about 50 – 60 at.% Cr.

In the context of this thesis we annealed samples of $\text{Fe}_{51}\text{Cr}_{49}$ and $\text{Fe}_{53.8}\text{Cr}_{46.2}$ at temperatures lying in the range $T = 1098 - 1133$ K. That means, since the Cr concentrations in our samples and the corresponding annealing temperatures are relatively high, the SRO parameter is definitely positive and thus the case of short-range clustering appears.

5.3 The σ -to- α phase transition

The transformation from the σ - into α -phase is a phase transition of first order since a change in the lattice structure is involved. The structures of the σ - and the α -phase are described in detail above.

The structure of the σ -phase is very complex. The unit cell is tetragonal and contains 30 atoms distributed over five inequivalent sites. Figure 5.3 shows that two sites are mainly occupied by Fe-atoms, while the other three are preferred by both Fe- and Cr-atoms.

The SRO parameter in the α - $\text{Fe}_{51}\text{Cr}_{49}$ and the α - $\text{Fe}_{53.8}\text{Cr}_{46.2}$ phase is repulsive. That means that the Fe- and Cr-atoms tend to build clusters.

This knowledge about the structures of the two phases allows us to draw the following conclusions about the phase transition: there definitely appears a rearrangement of the Fe- and Cr-atoms. Nevertheless, there will not occur a great mass transport; the atoms will not have to jump farther than to, say, the second nearest neighbor place. That is the reason why we do not expect the σ -to- α -phase transition (more precisely, the growth of the α -nuclei) to be diffusion controlled.

To study the σ -to- α phase transition (or vice versa) by means of Mößbauer spec-

troscopy one makes use of the fact that at room temperature ($T = 295$ K) the σ -phase is paramagnetic whereas the α -phase is magnetic [Hansen58]. The exact Curie points for σ -Fe-Cr and α -Fe-Cr depend on the Fe concentration. The Curie temperature for σ -Fe₅₃Cr₄₇ is $T_c \approx 55$ K and that for α -Fe₅₃Cr₄₇ is $T_c \approx 585$ K (cf. [Dubiel99]).

The two spectral parameters of Mößbauer spectroscopy, the hyperfine field and the isomer shift, change during the σ -to- α phase transition. This is due to the fact that during the transformation the neighborhood of the Fe nuclei changes. For this reason, there exist two methods to determine the kinetics of the σ -to- α phase transition:

1. fitting subspectra: a σ -to- α -transition spectrum consists of two subspectra which originate from the two phases. The spectrum of the σ -phase consists of a narrow distribution of lines due to the various sites (spectral area S_σ) and the one of the α -phase of a broadened sextet (spectral area S_α). Since the subspectra have thus different shape the amount of the α -phase in an overall Mößbauer spectrum can uniquely be determined:

$$A_\alpha = \frac{S_\alpha f_\sigma}{S_\alpha f_\sigma + S_\sigma f_\alpha}, \quad (5.1)$$

where f_α and f_σ denote the Lamb-Mößbauer factors for the α and the σ -phase, respectively. In [Cieślak00a] the following relation between the two Lamb-Mößbauer factors could be established:

$$f_\alpha = 0.87 \cdot f_\sigma. \quad (5.2)$$

Taking this into account (5.1) becomes

$$A_\alpha = \frac{S_\alpha}{S_\alpha + 0.87 \cdot S_\sigma}. \quad (5.3)$$

If one analyzes the σ -to- α -transformation spectra with this approach one gets values for A_α , that is the relative fraction of α -phase precipitated from the σ -phase. This data can then be fitted in terms of the Johnson-Mehl-Avrami-equation (cf. Section 3.2.1):

$$A_\alpha = 1 - \exp(- (t/\tau)^n). \quad (5.4)$$

2. average isomer shift: the subspectra of a spectrum do not only differ by their shape but also by the isomer shift. The difference in the isomer shift between the α - and the σ -spectrum is [Dubiel81]

$$\Delta IS = IS_\sigma - IS_\alpha \approx -0.11 \text{ mm/s}. \quad (5.5)$$

That means that the Fe-site charge-density in the σ -phase is ~ 0.06 s-like electron larger than in the α -phase.

The average isomer shift $\langle IS \rangle$ can be obtained directly by integrating the observed spectra. Assuming that $f_\sigma = f_\alpha$ the kinetics of the α -formation can finally be obtained by the following form of the Johnson-Mehl-Avrami-equation

$$\langle IS \rangle = (\langle IS_\sigma \rangle - \langle IS_\alpha \rangle) \exp(- (t/\tau)^n) + \langle IS_\alpha \rangle, \quad (5.6)$$

where $\langle IS_\alpha \rangle$ and $\langle IS_\sigma \rangle$ denote the average isomer shifts of the α - and the σ -phase, respectively.

5 *The system iron-chromium*

In the thesis at hand we have used the first approach (fitting subspectra). Even though the second approach (isomer shift) seems to be easier since one does not have to fit the spectra, it has the disadvantage that one does not obtain values for other spectral parameters like the relative intensities of the absorption lines. Thus fitting the subspectra yields more information. Nevertheless, the isomer shift approach can be very useful if the Mößbauer spectra are measured in-situ at temperatures above the α -Curie point, where fitting subspectra would be very difficult.

6 Results

The aim of this thesis was to study the kinetics of the σ -to- α phase transition in the system Fe-Cr. More precisely, we annealed samples of $\text{Fe}_{51}\text{Cr}_{49}$ at temperatures lying in the range 825 – 860°C and samples of $\text{Fe}_{53.8}\text{Cr}_{46.2}$ at 825 – 840°C.

The samples were prepared and annealed in a vacuum furnace as described in Section 4.2. They were alternately annealed for a specific time and ex-situ measured with the Mößbauer spectrometer, which is described in Section 4.1. With this approach we obtained Mössbauer spectra for every sample and temperature as a function of the annealing times.

Next, we want to present and discuss the transmission spectra of a specific sample annealed at a certain temperature to demonstrate the general fitting procedure and the subsequent interpretation of the results.

6.1 Fitting procedure and evaluation of the transmission spectra

To fit the transmission spectra we used the program RECOIL, a Mössbauer spectral analysis software for Windows (version 1.0) [Lagarec98], that was produced under the direction of D.G. Rancourt at the University of Ottawa.

The program is able to analyze various Mössbauer spectra using different models. For our purposes we made use of the Voigt-based fitting (VBF) method. A detailed and rigorous description of this method and its range of application can be found in [Rancourt91]. For a short overview we refer to [Lagarec98].

The VBF method is a tool to obtain hyperfine parameter distributions for multiple generalized sites in a Mössbauer spectrum. There are two types of such generalized sites: paramagnetic sites that can have a distribution of quadrupole splittings (QS) and magnetic sites that can have a distribution of magnetic hyperfine fields (HF).

The idea is to represent the hyperfine parameter distributions, that is the QS distribution (QSD) and the HF distribution (HFD), as sums of Gaussian components having different widths, positions, and weighting factors. In the case of a paramagnetic site this approach allows a linear coupling of the center shift to the QSD, whereas in the case of a magnetic site, the center shift and quadrupole shift can be linearly coupled to the HFD. In both cases the corresponding spectra turn out to be sums of Voigt profiles, i.e., convolutions of a Lorentzian and a Gaussian profile. For our purposes we do not need such linear couplings:

1. Modeling a Mössbauer lineshape, $Q(\nu)$, resulting from the presence of a QSD [Rancourt91, Section 2.2]:

6 Results

Let us write the QSD as a sum of Gaussians:

$$P(\Delta) = \sum_{i=1}^N p_i G(\Delta_{0i}, \sigma_{\Delta_{0i}}; \Delta), \quad (6.1)$$

where all variables and their meaning are listed in Table 6.2. The elemental quadrupole doublet is the sum of two Lorentzians:

$$D(\Delta; \nu) = \sum_{k=-1}^{+1} h_k L(\delta + k\Delta/2, \gamma; \nu). \quad (6.2)$$

The final Möbbauer lineshape, $Q(\nu)$, is given by the convolution of these functions:

$$Q(\nu) = \int_{-\infty}^{+\infty} D(\Delta; \nu) P(\Delta) d\Delta. \quad (6.3)$$

Thus finally $Q(\nu)$ turns out to be a sum of $2N$ Voigt profiles:

$$Q(\nu) = \sum_{i=1}^N p_i \sum_{k=-1}^{+1} h_k V(\delta + k\Delta_{0i}/2, |k/2|\sigma_{\Delta_{0i}}, \gamma; \nu). \quad (6.4)$$

2. Modeling a Möbbauer lineshape, $H(\nu)$, resulting from the presence of a HFD [Rancourt91, Section 2.3]:

Now we write the HFD as a sum of Gaussians:

$$P(z) = \sum_{i=1}^N p_i G(z_{0i}, \sigma_{z_{0i}}; z), \quad (6.5)$$

where all variables and their meaning can again be looked up in Table 6.2. The elemental sextet is the sum of six Lorentzians:

$$S(z; \nu) = \sum_{k=1}^6 L(\omega_k, \gamma, h_k; \nu), \quad (6.6)$$

where ω_k , $k = 1, \dots, 6$ denote the positions of the six lines of a Möbbauer sextet:

$$\begin{aligned} \omega_1 &= \delta - (Z + 3)z/2 := \delta - A_1 z, \\ \omega_2 &= \delta - (Z + 1)z/2 := \delta - A_2 z, \\ \omega_3 &= \delta - (Z - 1)z/2 := \delta - A_3 z, \\ \omega_4 &= \delta + (Z - 1)z/2 := \delta - A_4 z, \\ \omega_5 &= \delta + (Z + 1)z/2 := \delta - A_5 z, \\ \omega_6 &= \delta + (Z + 3)z/2 := \delta - A_6 z. \end{aligned} \quad (6.7)$$

6.1 Fitting procedure and evaluation of the transmission spectra

The final Mößbauer lineshape, $H(\nu)$, is given by the convolution of $P(z)$ and $S(\nu)$:

$$Q(\nu) = \int_{-\infty}^{+\infty} S(z; \nu) P(z) dz. \quad (6.8)$$

Note that $S(\nu)$ also depends on z via ω_k . Thus finally $H(\nu)$ turns out to be a sum of $6N$ Voigt profiles:

$$H(\nu) = \sum_{i=1}^N p_i \sum_{k=1}^6 h_k V(\delta + A_k z_{0i}, |A_k| \sigma_{z_{0i}}, \gamma; \nu), \quad (6.9)$$

where A_k is defined via (6.7).

Variable	Definition
γ	Lorentzian FWHM
h_k, h_{\pm}	Lorentzian heights of the six lines ($k = 1, \dots, 6$) resp. of the two lines ($k = +, -$)
δ	center shift of a doublet or sextet
Δ	quadrupole splitting (QS) parameter
Δ_0	center of Gaussian component of a QSD
z	nuclear Zeeman splitting parameter
z_0	center of Gaussian component of a HFD
Z	ratio of ^{57}Fe nuclear g -factors, ground state to excited state
$P(\Delta), P(z)$	hyperfine parameter distribution of Δ resp. z
$D(\Delta; \nu), S(z; \nu)$	elemental Lorentzian ^{57}Fe quadrupole doublet resp. hyperfine sextet
p_i	weight factors
$\sigma_{\Delta}, \sigma_z$	Gaussian widths of Gaussian components of a QSD resp. HFD
$L(\vec{a}; x)$	Lorentzian function, where $\vec{a} = (\text{center}, \text{width})$ and x denotes the argument
$G(\vec{a}; x)$	Gaussian function, where $\vec{a} = (\text{center}, \text{width})$ and x denotes the argument
$V(\vec{a}; x)$	Voigt function, where $\vec{a} = (\text{center}, \text{Gaussian-width}, \text{Lorentzian-width})$ and x denotes the argument

Table 6.2: Defintions of the variables in the context of hyperfine parameter distributions.

We now want to take a look at the measured transmission spectra for the sample $\text{Fe}_{51}\text{Cr}_{49}$ annealed at $T = 840^\circ\text{C}$ corresponding to the different annealing times, see Figure 6.1. The spectra (counts per channel) were recorded by the Mößbauer spectrometer. Subsequently, all spectra were folded and analyzed with the program RECOIL.

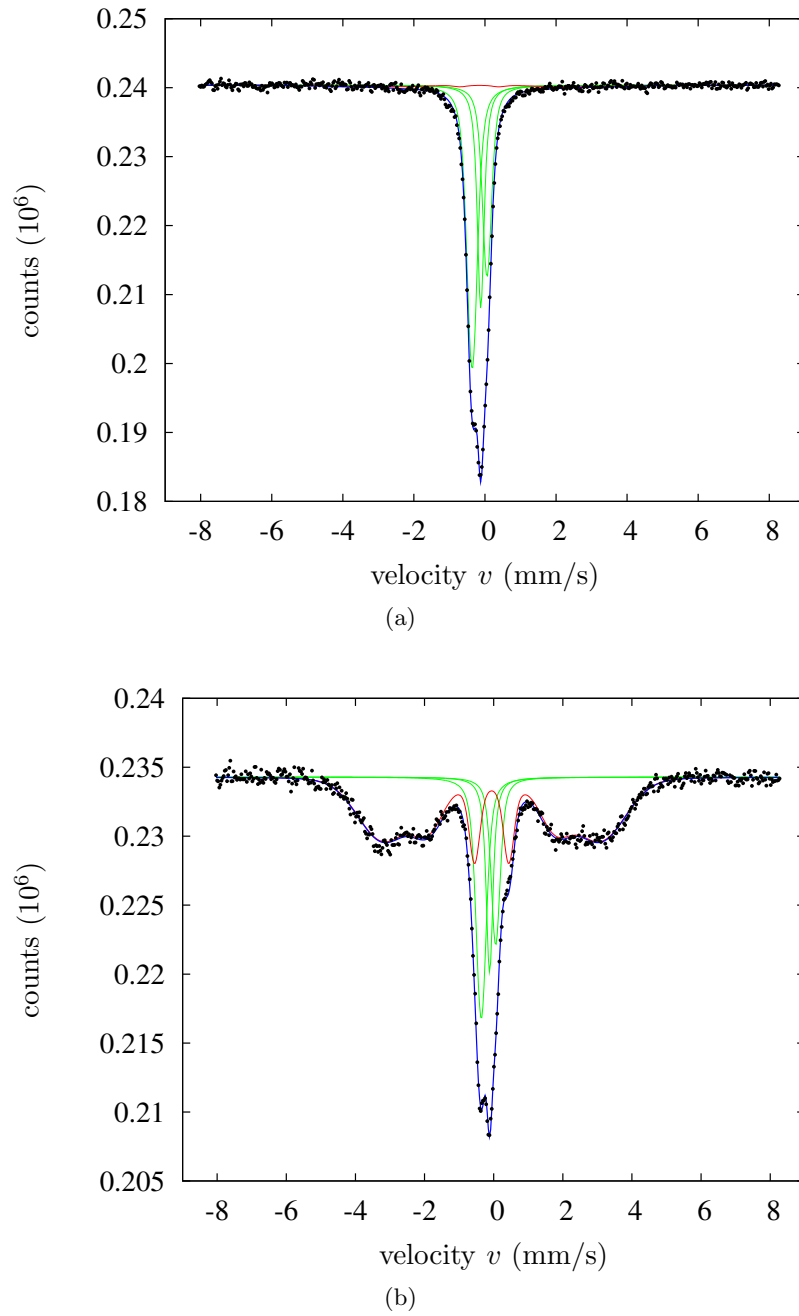


Figure 6.1: Mößbauer transmission spectra of the sample $\text{Fe}_{51}\text{Cr}_{49}$ at $T = 840^\circ\text{C}$ for different annealing times: (a) $t = 5$ min ($A_\alpha = 3.89\%$), (b) $t = 21$ min ($A_\alpha = 66.06\%$). A_α constitutes the corrected α -fraction present in the sample (cf. equation (5.3)). The fit (blue) is the sum of the three QSD sites (green) and the HFD site (red).

6.1 Fitting procedure and evaluation of the transmission spectra

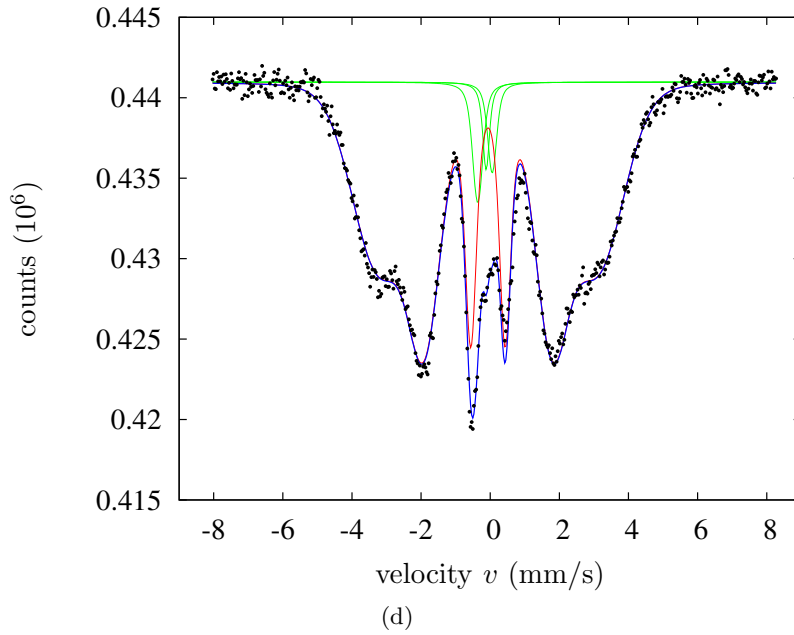
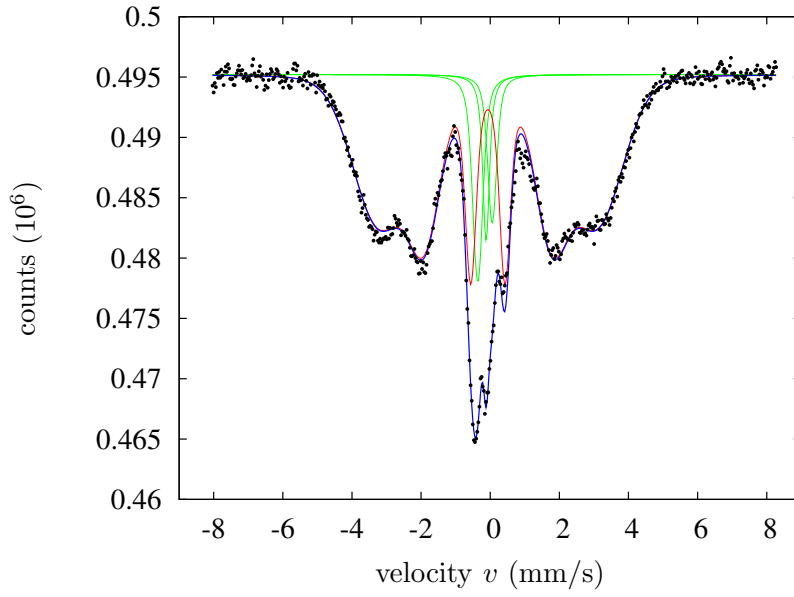


Figure 6.1: Mössbauer transmission spectra of the sample $\text{Fe}_{51}\text{Cr}_{49}$ at $T = 840^\circ\text{C}$ for different annealing times: (c) $t = 24$ min ($A_\alpha = 85.71\%$), (d) $t = 27$ min ($A_\alpha = 93.48\%$). A_α constitutes the corrected α -fraction present in the sample (cf. equation (5.3)). The fit (blue) is the sum of the three QSD sites (green) and the HFD site (red).

6 Results

To fit a spectrum we used the VBF method which was presented in detail above. In our case one Mößbauer spectrum consists of two subspectra originating from the σ - and the α -phase, respectively. Since the σ -phase is a paramagnetic one, we used three paramagnetic sites (QSD's) to fit that part corresponding to this phase. The α -phase, on the other hand, is magnetic and thus we used one magnetic site (HFD) to fit the part coming from this phase. The two parts should finally add up to give the overall spectrum.

The fact that the subspectrum corresponding to the σ -phase is fitted by three QSD sites instead of five, as it would be indicated by the fact that there exist five inequivalent sites in the unit cell (cf. Section 5.1), is just because of phenomenological reasons. It shows that these three QSD sites are enough since they fit the spectrum within the precision of measurements.

To summarize, each transmission spectrum is fitted with 4 sites (3 QSD sites, 1 HFD site), where each site consists of only one Gaussian component ($N = 1$). The procedure of fitting the sequence of spectra corresponding to the sample $\text{Fe}_{51}\text{Cr}_{49}$ and the temperature $T = 840^\circ\text{C}$ was as follows:

1. first, one arbitrary spectrum of the row (where the sample consists of approximately 50% α -phase) was fitted, where the following fit parameters were free:
 - parameters corresponding to each of the three QSD sites: δ , area, $\langle\Delta\rangle = \langle QS \rangle$ (average QS), and σ_Δ (the last two correspond to the Gaussian component of the site) and
 - parameters corresponding to the HFD site: δ , area, $h_2/h_3 = A_2/A_3$, $\langle z \rangle$ (average Zeeman splitting, or alternatively the average magnetic field $\langle H \rangle$), and σ_z (the last two again contribute to the Gaussian component of the site).

The following parameters were fixed during the fitting process:

- parameters corresponding to each of the three QSD sites: $h_-/h_+ = A_-/A_+ = 1$ and
 - parameters corresponding to the HFD site: $h_1/h_3 = A_1/A_3 = 3$.
2. The values for the parameters obtained by step 1 were taken to fit all other spectra of the row, where now only the following parameters were left free (the others were fixed at the values obtained in step 1.):
 - parameter corresponding to each of the three QSD sites: area and
 - parameters corresponding to the HFD site: δ , area, $h_2/h_3 = A_2/A_3$, $\langle z \rangle$ (average Zeeman splitting, or alternatively the average magnetic field $\langle H \rangle$), and σ_z .

For the definitions of all variables we again refer to Table 6.2.

Regarding the relative intensity of the absorption lines A_2/A_3 one has to note that it is useful to let this parameter be fixed, that is equal to 2, if the amount of the α -phase in the sample is low, e.g. less than 20%. If the amount gets higher one should let

6.1 Fitting procedure and evaluation of the transmission spectra

A_2/A_3 be a free fit parameter, since our sample shows a presence of texture and thus the value can be between 0 and 4 (cf. Section 2.2.4). Moreover, the Lorentzian FWHM $\gamma = 0.097$ mm/s is fixed during all fitting processes, since we assumed the broadening of the spectra due to thickness effects to be negligible.

The values of the parameters that were received after step 1. of the fitting procedure and left fixed during step 2. are listed in Table 6.3. Concerning the values of the HFD

Parameter (units)	QSD site 1	QSD site 2	QSD site 3
δ_0 (mm/s)	-0.360	-0.118	0.058
$\langle\Delta\rangle$ (mm/s)	0.021	0.0002	0.011
σ_Δ (mm/s)	0.204	0.081	0.162

Table 6.3: Values of the parameters of the three QSD sites.

site and the QSD sites received during the fitting process of each spectrum (step 2.) we refer to Table 6.4.

Type of site	Parameter (units)	Spectrum			
		(a)	(b)	(c)	(d)
QSD site 1	Area (%)	44.3	16.8	7.2	3.4
QSD site 2	Area (%)	27	10.5	4.7	2.3
QSD site 3	Area (%)	25.3	9.8	4.2	1.8
HFD site	Area (%)	3.4	62.9	83.9	92.6
	δ_0 (mm/s)	-0.157	-0.058	-0.067	-0.064
	A_2/A_3	2	1.28	1.78	2.306
	$\langle H \rangle$ (T)	19.4	19.4	19.4	19.51
	σ_H (T)	5.4	4.4	4.49	4.58

Table 6.4: Values of the parameters of the three QSD sites and of the HFD site for the four spectra shown in Figure 6.1.

The area of the HFD site and the areas of the QSD sites add up to 100%. To get the fraction A_α of the α -phase present in the sample one can not just take the area of the HFD site directly. Rather, we have to take the different Lamb-Mössbauer factors of the σ - and α -phase into account and thus we will use (5.3) to calculate A_α . Here S_α denotes the area of the HFD site and S_σ the sum of the areas of the three QSD sites.

It can be seen in Table 6.5 that there is no significant dependence of the mean magnetic field $\langle H \rangle$ on the annealing times, i.e. on the amount of precipitated α -phase in the sample.

However, the values of the ratio of the absorption lines A_2/A_3 increase from 1 to 3 as the annealing times increase.

The fraction A_α obviously depends on the annealing times. This dependence is illustrated in Figure 6.2. The data was fitted in terms of the Johnson-Mehl-Avrami-

6 Results

Time t (min)	A_α (%)	$A2/A3$	$\langle H \rangle$ (T)
5	3.9(20)	-	-
9	5.0(20)	-	-
11	6.5(20)	-	-
13	10.8(11)	-	-
16	28.5(20)	0.80(44)	19.5(11)
18	45.8(15)	0.83(22)	19.05(47)
21	66.1(10)	1.28(11)	19.41(21)
24	85.7(6)	1.779(61)	19.45(11)
27	93.5(6)	2.306(64)	19.508(100)
30	96.7(7)	2.726(81)	19.42(11)

Table 6.5: Values of the ratio $A2/A3$ and the mean magnetic field $\langle H \rangle$ of the sample $\text{Fe}_{51}\text{Cr}_{49}$ at $T = 840^\circ\text{C}$ for different annealing times (i.e. different α -fractions A_α). The sign - indicates that the fit parameter has been fixed.

Kolmogorov equation (cf. Section 3.2.1)

$$A_\alpha = 1 - \exp\left(- (t/\tau)^n\right). \quad (6.10)$$

The results for the parameters n and τ are

$$\begin{aligned} n &= 4.2 \pm 0.2, \\ \tau &= 20.6 \pm 0.2 \text{ min.} \end{aligned}$$

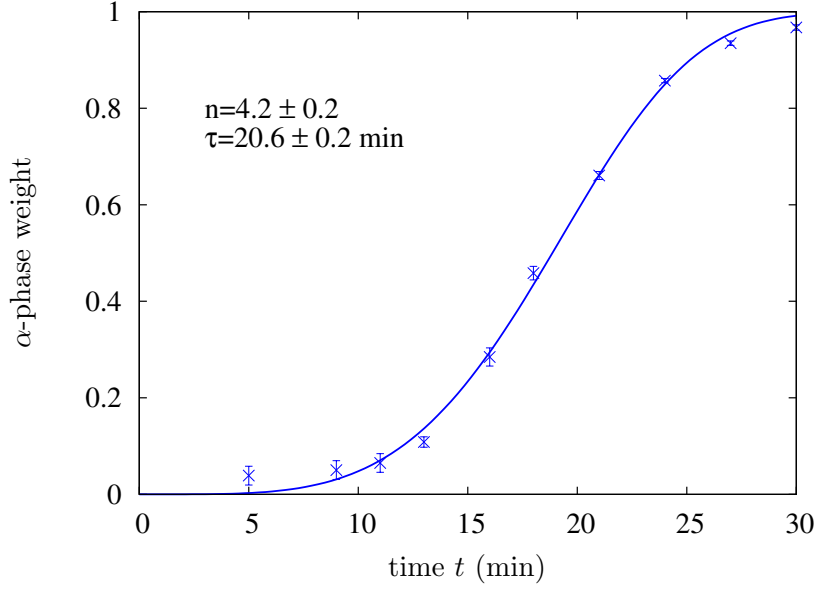
6.2 Kinetics of the phase transformation

In the way described above we evaluated the kinetics of the samples $\text{Fe}_{51}\text{Cr}_{49}$ and $\text{Fe}_{53.8}\text{Cr}_{46.2}$ for different annealing temperatures. The resulting data are shown in Figure 6.3 and Figure 6.4, respectively. The solid lines in the figures again represent the best-fits to the data in terms of the Johnson-Mehl-Avrami-Kolmogorov equation. Concerning Figure 6.3 one may observe that the lines corresponding to the three lowest temperatures 825°C , 830°C , and 835°C systematically differ from the other ones. This is due to the fact that the samples of $\text{Fe}_{51}\text{Cr}_{49}$ annealed at these three temperatures unfortunately have a different sample history than the samples corresponding to the higher temperatures.

Thus we got values for the best-fit kinetics parameters n and τ corresponding to the different Fe-content in the sample and to the various annealing temperatures.

6.2.1 Activation energy

A useful reference for this section turned out to be [Mittemeijer92].

Figure 6.2: Kinetics of the transformation in the sample $\text{Fe}_{51}\text{Cr}_{49}$ at $T = 840^\circ\text{C}$.

T ($^\circ\text{C}$)	$\text{Fe}_{51}\text{Cr}_{49}$		$\text{Fe}_{53.8}\text{Cr}_{46.2}$	
	n	τ (min)	n	τ (min)
825	1.3(1)	304.7(13)	1.63(5)	35.7(5)
827	-	-	2.1(3)	36.9(14)
830	2.1 (3)	44.3(14)	3.2(3)	12.5(2)
835	2.3(2)	19.7(3)	3.3(2)	7.5(1)
840	4.2(2)	20.6(2)	3.2(5)	4.2(2)
845	5.0(3)	14.7(2)	-	-
850	2.3(3)	7.2(3)	-	-
855	3.9(4)	4.3(1)	-	-
860	3.4(5)	1.8(1)	-	-

Table 6.6: Values of the parameters n and τ corresponding to the different Fe-content in the sample and to the various annealing temperatures. The sign - indicates that the sample has not been annealed at the corresponding temperature.

As discussed in Section 3.2.1 the amount transformed into α is given by the JMAK-equation

$$A_\alpha(t) = 1 - \exp\left(-\frac{4\pi}{3} \int_0^t I(\tau)(r(t-\tau))^3 d\tau\right). \quad (6.11)$$

Here $4\pi(r(t-\tau))^3/3$ denotes the volume of a particle at time t which has been nucleated at the time τ and $I(\tau)$ determines the nucleation rate per unit volume at time τ .

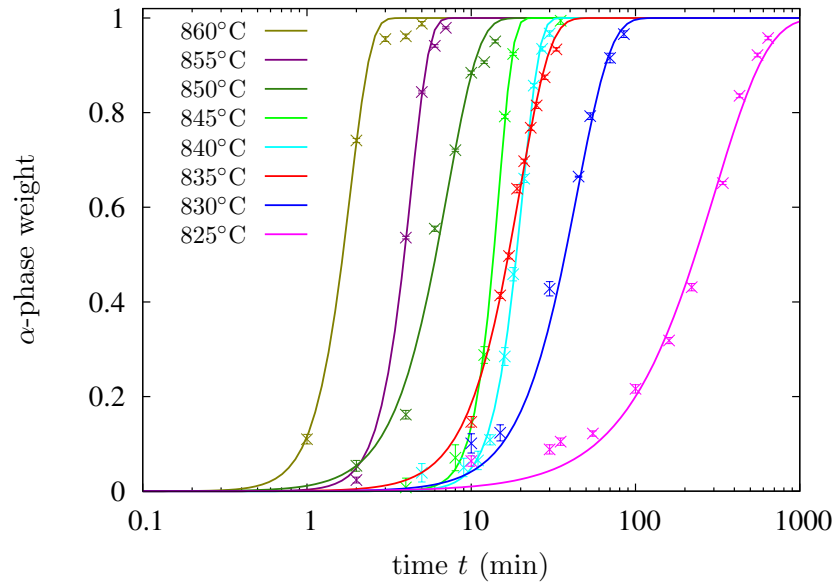


Figure 6.3: Kinetics of the transformation in the composition $\text{Fe}_{51}\text{Cr}_{49}$ at different annealing temperatures.

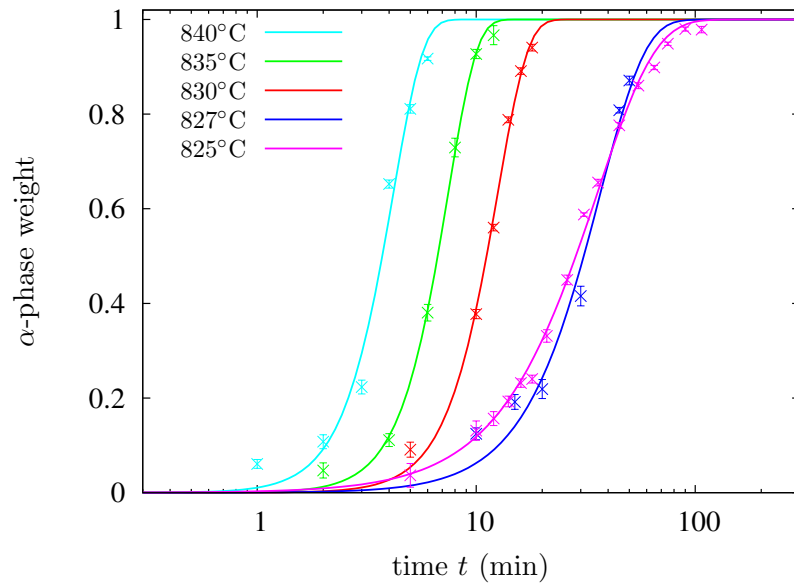


Figure 6.4: Kinetics of the transformation in the composition $\text{Fe}_{53.8}\text{Cr}_{46.2}$ at different annealing temperatures.

Thus there are two main processes contributing to the transformation rate: a growth mechanism of the particles and a nucleation mechanism. Let us impose an Arrhenius-type temperature dependence on both, i.e., on the radius $r(t - \tau)$ (growth) and the nucleation rate per unit volume $I(\tau)$ (nucleation). That means we write

$$I(\tau) = I_0(\tau) \exp\left(-\frac{E_N}{k_B T}\right), \quad (6.12)$$

$$r(t - \tau) = v \exp\left(-\frac{E_G}{k_B T}\right)(t - \tau), \quad (6.13)$$

where $v \exp(-E_G/(k_B T))$ denotes the “velocity” of the growth, k_B Boltzmann’s constant and E_N and E_G can be considered as the activation energy of nucleation and growth, respectively. Then (6.11) becomes

$$f_\alpha(t) = 1 - \exp\left(-\frac{4\pi}{3} v^3 \exp\left[-\frac{E_N + 3E_G}{k_B T}\right] \int_0^t I_0(\tau)(t - \tau)^3 d\tau\right). \quad (6.14)$$

Comparing this expression with the equation

$$A_\alpha = 1 - \exp\left(-\left(t/\tau\right)^n\right), \quad (6.15)$$

yields the following Arrhenius-relation for the parameter τ :

$$\tau(T) = \tau_0 \exp\left(\frac{E}{k_B T}\right), \quad (6.16)$$

where E can be considered as an effective activation energy

$$E = E_N + 3E_G. \quad (6.17)$$

The value for E can be read off by making an Arrhenius plot, which is shown in Figure 6.5. Note that the activation energy can depend on the degree of transformation since the governing mechanisms can change. In our case it seems reasonable to assume that near the critical temperature ($T = 821^\circ\text{C}$) there happens a change of the nucleation mechanism (cf. Section 6.2.2). The values for τ at 825°C and 827°C seemingly also show a critical behavior and are therefore not used as fitting data. The remarkable thing about the fit concerning the remaining values for τ is that we assumed for both compositions $\text{Fe}_{51}\text{Cr}_{49}$ and $\text{Fe}_{53.8}\text{Cr}_{46.2}$ the same value for E and only with τ_0 being different the fits are seen to be rather good.

Note that above deviation of the temperature dependence of τ assumed a constant difference in the free energies of α and σ (which is the thermodynamic driving force of the transformation). This is permissible far away from the critical temperature, but near it kinetics can not be expected to follow a simple Arrhenius relation, which is also visible in Figure 6.5.

We ignored the different sample history (and the resulting deviation of the values for τ) of the samples of $\text{Fe}_{51}\text{Cr}_{49}$ annealed at 830°C and 835°C . The fact that τ is a

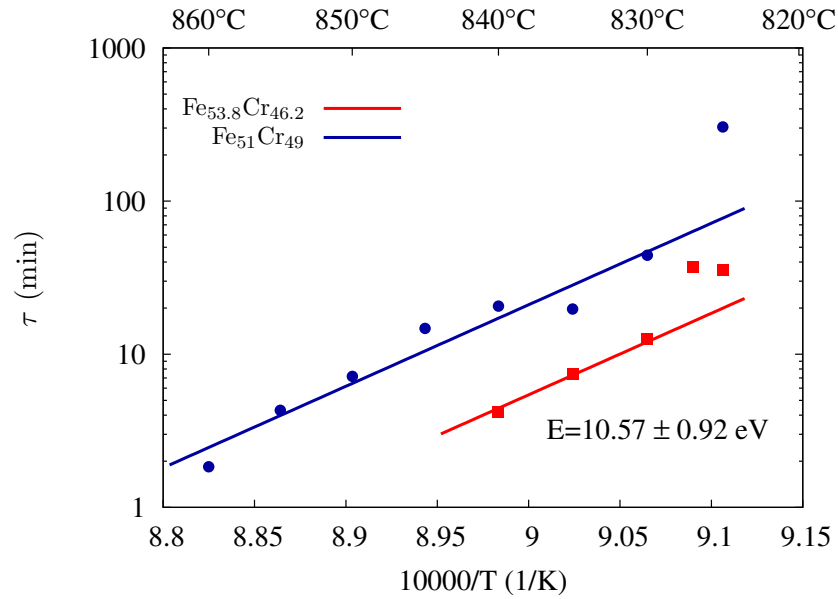


Figure 6.5: Arrhenius plot of time constant of the transformation. The errorbars are not visible since they are smaller than the symbols.

function of the sample history follows from the observation that the fit is very often far outside the estimated error bars.

The value obtained for the effective activation energy E is

$$E = 10.57 \pm 0.92 \text{ eV.}$$

This seems to be a relatively high activation energy. Since growth happens by atomic movement, its activation energy E_G should be on the order of magnitude of the activation energy of diffusion in a grain boundary, which is usually below 1 eV. We therefore have good reasons to conclude that the dominant part contributing to E is the activation energy of nucleation E_N . A high value for E_N means that the nucleation rate per unit volume $I(\tau)$ is low.

In this context it would be interesting to measure the relative change of the size and the number of grains in a sample. This could be established by investigating a specific sample with a low and a high transformed fraction by X-ray diffraction methods. We would expect that the results show no essential increase of the number of grains but definitely an increase of the volume of the particles as the α -fraction in the sample grows.

For comparison, in [Kuwano85a] an effective activation energy of $E = 2.0$ eV for the α -to- σ -phase transition in Fe-Cr could be obtained.

In [Blachowski00a] it was reported that in an Ti-doped coarse-grained FeCr alloy this activation energy can change. For Ti-doped Fe_{53.8}Cr_{46.2} with a Ti-content less

than 1.5 at.% the value for E is lower than the one for a pure FeCr alloy. That is the presence of titanium accelerates the formation of the σ -phase. For a Ti-content greater than 1.5 at.% the transformation from the α - into the σ -phase is retarded.

In [Blachowski00b] Blachowski et al. observed a retardation of the σ -phase formation in an 1 at.% Al-doped FeCr alloy.

Elmer et al. [Elmer07] investigated the σ -phase formation from ferrite (bcc) in duplex stainless steel. They measured this transformation by using synchrotron radiation during an isothermal annealing at temperatures ranging from 700°C to 850°C. To determine the activation energy they restricted themselves to the data obtained for the two lowest temperatures, 700°C and 750°C. This is due to the fact that for higher temperatures a change in the type of the nucleation mechanism could be observed (corresponding to a change of the Avrami exponent n). The value for the activation energy varies between 3.70 eV and 4.99 eV (depending on the σ -fraction transformed). This values are seen to be much lower than the value we obtained for the σ -to- α phase transition in Fe-Cr. This is maybe because of the fact that we obtained the value for E from the values for τ at the temperatures between 860°C and 830°C, which are relatively near to the critical temperature of 821°C, whereas Elmer et al. obtained their value for the activation energy from the data at 700°C and 750°C, which differ much more from the critical temperature of 860°C. Apart from that, duplex stainless steel is a much more complex material than Fe-Cr and thus one has to be cautious about a direct comparison.

6.2.2 Avrami-Exponent

The values of the Avrami-exponent n corresponding to different annealing temperatures and Fe-content in the sample are listed in Table 6.6 and shown graphically in Figure 6.6.

As mentioned in Section 3.2.1 the Avrami-exponent n is a characteristic constant of the type of the nucleation mechanism. The relative Fe- and Cr-concentration of the α -phase precipitated is the same as in the σ -matrix-phase. Therefore there occurs no mass transport, thus the growth of the α -nuclei can be considered to be interface controlled rather than diffusion controlled (cf. Section 5.3). Moreover, let us impose a 3-dimensional growth on the nuclei. Then the value for n gives us information about the nucleation rate and thus on the underlying transformation mechanism, see Table 6.7.

If we take a look at Figure 6.6 we observe that in the temperature range $\sim 825 - 830^\circ\text{C}$, i.e., for temperatures near the critical temperature 821°C, the Avrami-exponent n lies between 1 and 2. On the other hand, for temperatures above 840°C, n seems to be between 3 and 4. Thus we conclude that for near-critical temperatures there occurs heterogeneous nucleation (nucleation at grain boundaries and edges). For higher temperatures, however, the mechanism of nucleation looks homogeneous.

In [Elmer07] it was reported that for the ferrite to σ -phase transformation (already mentioned above) the Avrami exponent n and thus the transformation mechanism significantly depends on the amount of σ -phase transformed. For low σ -fractions n is found to be about 7.0, while for high σ -fractions the Avrami exponent n takes values

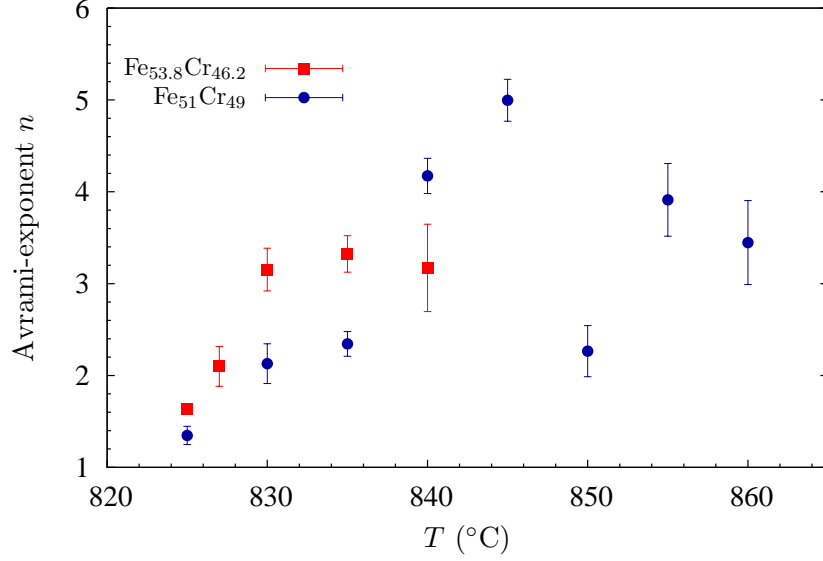


Figure 6.6: Avrami exponent n of the compositions $\text{Fe}_{51}\text{Cr}_{49}$ and $\text{Fe}_{53.8}\text{Cr}_{46.2}$ for different annealing temperatures.

n	Conditions	Type
> 4	Increasing nucleation rate	homogeneous
4	Constant nucleation rate	
3 – 4	Decreasing nucleation rate	
3	Zero nucleation rate	
2	Grain edge nucleation	heterogeneous
1	Grain boundary nucleation	

Table 6.7: Values of the Avrami exponent n .

of approximately 0.75.

6.2.3 Relative intensities of the absorption lines

As discussed in Section 2.2.4 the intensity ratios of the absorption lines of a Mößbauer spectrum depend on the angle θ enclosed by the direction of propagation of the γ -ray photon and the principal axis of the magnetic field. More precisely, the ratio of the absorption line A_2 and A_3 takes the value

$$\frac{A_2}{A_3} = \frac{4 \sin^2 \theta}{1 + \cos^2 \theta}.$$

This means that the ratio A_2/A_3 can vary from 0 ($\theta = 0^\circ$, orientation of easy magnetization “out-of-plane”) to 4 ($\theta = 90^\circ$, orientation of easy magnetization “in-plane”).

Figure 6.7 shows the values of A_2/A_3 depending on the α -phase weight for the samples $\text{Fe}_{51}\text{Cr}_{49}$ and $\text{Fe}_{53.8}\text{Cr}_{46.2}$. The following two observations can be made: first, A_2/A_3 depends on the Fe-content in the sample. It seems to be higher for compositions with larger atom-percent iron. Second, with increasing α -phase fraction the value of A_2/A_3 rises from 1 to 3. That means that if the fraction of α -phase in the sample $\text{Fe}_{51}\text{Cr}_{49}$ ($\text{Fe}_{53.8}\text{Cr}_{46.2}$) is less than $\sim 80\%$ ($\sim 90\%$) the magnetization of the sample prefers to be “out-of-plane”, for higher amounts of the α -phase it changes to “in-plane”.

In particular the latter observation is rather astonishing. For pure α -Fe it is well known [Weißmantel95, Section 10.8] that the easy axes of magnetization are the family of $\langle 100 \rangle$ directions. Additionally one knows that in the case of a thin Fe-foil the actual directions of magnetization prefer to lie “in-plane”. Thus naively one would assume that A_2/A_3 is (independent of the fraction of α -phase precipitated) always about 3. For this reason the observed change in the orientation of magnetization from “out-of-plane” to “in-plane” is interesting and worth being studied in detail in future work.

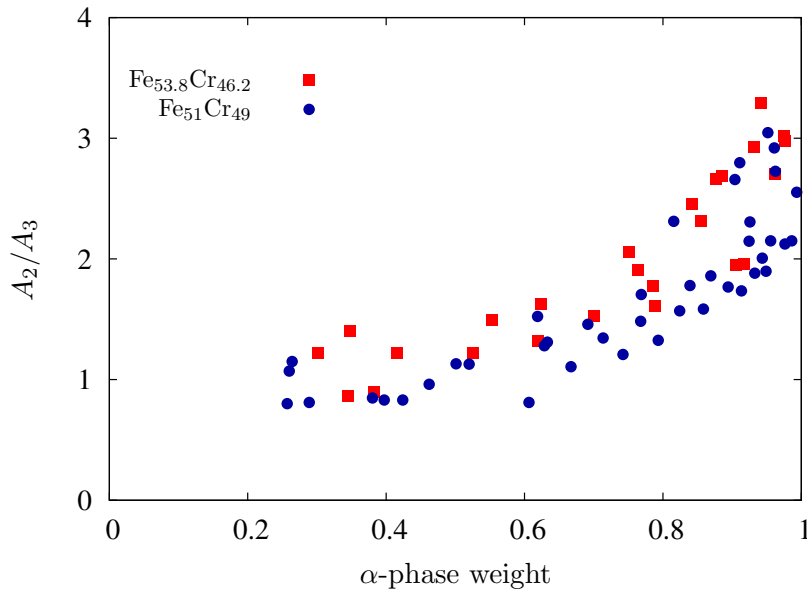


Figure 6.7: Ratio of the absorption lines A_2/A_3 of the compositions $\text{Fe}_{51}\text{Cr}_{49}$ and $\text{Fe}_{53.8}\text{Cr}_{46.2}$ for different annealing times.

6.2.4 Mean magnetic field

In Figure 6.8 the mean magnetic field $\langle H \rangle$ of the samples $\text{Fe}_{51}\text{Cr}_{49}$ and $\text{Fe}_{53.8}\text{Cr}_{46.2}$ are shown. Obviously there is no significant dependence of the value $\langle H \rangle$ on the amount

6 Results

of α -phase present in the sample (i.e., on the annealing time). However, the mean magnetic field $\langle H \rangle$ is seen to be larger in samples with higher Fe-content. This is not surprising, since the number of Fe-nearest neighbors of each atom in the lattice and therefore the magnetic field at the location of the nucleus increases.

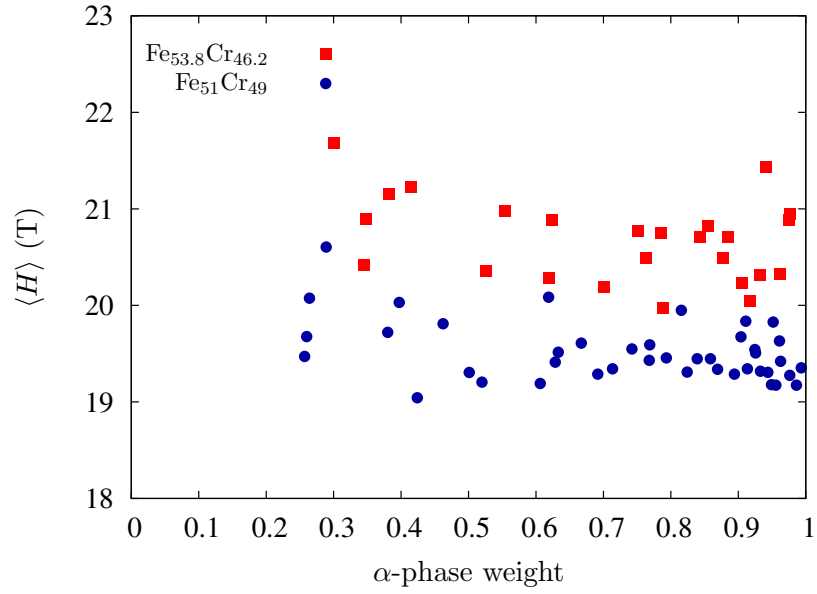


Figure 6.8: Mean magnetic field $\langle H \rangle$ of the compositions $\text{Fe}_{51}\text{Cr}_{49}$ and $\text{Fe}_{53.8}\text{Cr}_{46.2}$ for different annealing times.

7 Summary and conclusion

The subject of the thesis at hand was the σ -to- α -phase transition in the system Fe-Cr. The α -phase constitutes the high-temperature bcc-phase, while the σ -phase is stable at temperatures lower than 821°C and if the Cr-content lies in the range 43–49 at%. The phase transformation was studied by means of ^{57}Fe Mößbauer spectroscopy utilizing the fact that the σ -phase is paramagnetic and the α -phase is ferromagnetic at room temperature.

The degree of phase transformation, i.e., the fraction transformed from σ into α , is a function of time, temperature, and amount of Fe-content in the sample. Thus we annealed samples of different composition, i.e., $\text{Fe}_{51}\text{Cr}_{49}$ and $\text{Fe}_{53.8}\text{Cr}_{46.2}$, at different temperatures higher than the critical temperature of 821°C. In that way we obtained a sequence of Mößbauer spectra for each temperature and composition corresponding to the different annealing times. These spectra, which constitute a linear combination of a set of doublets (paramagnetic σ -phase) and a sextet (ferromagnetic α -phase) were fitted to determine the transformed fraction.

For the analysis of the kinetics of the phase transition we made use of the Johnson-Mehl-Avrami-Kolmogorov-equation

$$A_{\alpha}(t) = 1 - \exp\left(- (t/\tau)^n\right), \quad (7.1)$$

where A_{α} denotes the amount of α -phase present in the sample. The σ -to- α -phase transition turned out to proceed faster for a higher Fe-content. Moreover, values for the Avrami exponent n , which is an characteristic constant of the type of nucleation process, could be obtained. For both compositions n lies between 1 and 2 for annealing temperatures near the critical temperature of 821°C and rises up to about 4 for higher temperatures. Thus we conclude that for temperatures near the critical temperature the nucleation mechanism is heterogeneous and for higher temperatures it becomes homogeneous.

We also obtained values for τ , the time constant. If one imposes an Arrhenius relation on τ one can determine the activation energy, which in our case is the same for both compositions:

$$E = 10.57 \pm 0.92 \text{ eV.}$$

This activation energy can be considered an effective activation energy, i.e., a sum of energies which are due to the nucleation and growth mechanisms happening during the transformation, also absorbing effects of the changing driving force. Since E is relatively high we concluded that the main part contributing to E is the activation energy for nucleation E_N . A high value for E_N implies a low nucleation rate per unit

7 Summary and conclusion

volume. An interesting issue for a possible future project would hence be to investigate the grain sizes in a sample by X-ray diffraction methods. We would expect that the number of nuclei does not increase essentially as the α -fraction gets higher, whereas the size of the grains should grow rapidly.

Departing from the investigation of the phase transition, other interesting physical phenomena could be observed. From the fitting procedure of the spectra we got values for spectral parameters such as the mean magnetic field $\langle H \rangle$ and the relative intensity ratios of the absorption lines A_2/A_3 resulting from the sextet.

It turned out that the value for $\langle H \rangle$ is not a function of the degree of transformation, but of the composition, i.e., of the Fe-content in the sample. The mean magnetic field takes a larger value for compositions with higher Fe-content, that is in our investigations $\text{Fe}_{53.8}\text{Cr}_{46.2}$.

From the ratio of the areas of the hyperfine lines A_2/A_3 one can draw conclusions about the orientation of easy magnetization in the sample. The value for A_2/A_3 can range from 0 (orientation of the axis of magnetization “out-of-plane”) to 4 (orientation of the axis of magnetization “in-plane”). We had expected a value about 3 nearly independent of the fraction transformed. Instead we made the quite astonishing observation that A_2/A_3 depends strongly on the α -phase weight in the sample. It rises from 1 to 3, which means that the preferred orientation of magnetization changes from “out-of-plane” to “in-plane” as the α -fraction increases. This phenomenon seems to have not been observed before and hence should be investigated in the future, e.g., by computer simulations.

As one can see, the investigation of the σ -to- α -phase transition brought in many interesting results. On the other hand from this study also a few issues have arisen, which can be considered worth being explored in prospective future work.

Bibliography

- [Avrami39] Avrami, M. *Kinetics of phase change. I General theory*. The Journal of Chemical Physics 7, 1103 (1939).
- [Avrami40] Avrami, M. *Kinetics of Phase Change. II Transformation-Time Relations for Random Distribution of Nuclei*. The Journal of Chemical Physics 8, 212 (1940).
- [Avrami41] Avrami, M. *Kinetics of phase change. III Granulation, phase change, and microstructure*. The Journal of Chemical Physics 9, 177 (1941).
- [Bain23] Bain, E. *Nature of Solid Solutions*. Chemical and Metallurgical Engineering 28, 21 (1923).
- [Bergman54] Bergman, G. and Shoemaker, D. *The determination of the crystal structure of the phase in the iron-chromium and iron-molybdenum systems*. Acta Crystallographica 7, 857 (1954).
- [Blachowski99] Blachowski, A., Cieślak, J., Dubiel, S., and Sepiol, B. *Kinetics of the sigma-phase formation in an (Fe_{53.8}Cr_{46.2})-0.1 at.% Ti alloy*. Phil. Mag. Lett. 79, 87 (1999).
- [Blachowski00a] Blachowski, A., Cieślak, J., Dubiel, S., and Sepiol, B. *Effect of titanium on the kinetics of the σ -phase formation in a coarse-grained Fe-Cr alloy*. Intermetallics 8, 963 (2000).
- [Blachowski00b] Blachowski, A., Dubiel, S., Zukrowski, J., Cieślak, J., and Sepiol, B. *On the kinetics of the α - σ phase transformation in an Al-doped Fe-Cr alloy*. Journal of Alloys and Compounds 313, 182 (2000).
- [Bonny09] Bonny, G., Erhart, P., Caro, A., et al. *The influence of short range order on the thermodynamics of Fe-Cr alloys*. Modelling and Simulation in Materials Science and Engineering 17, 025006 (2009).
- [Breit36] Breit, G. and Wigner, E. *Capture of slow neutrons*. Physical Review 49, 519 (1936).
- [Cieślak98] Cieślak, J. and Dubiel, S. *Nucleation and growth versus spinodal decomposition in Fe-Cr alloys: Mössbauer-effect modelling*. Journal of Alloys and Compounds 269, 208 (1998).

Bibliography

- [Cieślak99] Cieślak, J., Dubiel, S., and Sepiol, B. *In situ Mössbauer-effect study of the kinetics of the sigma-phase formation*. Solid State Communications 111, 613 (1999).
- [Cieślak00a] Cieślak, J., Dubiel, S., and Sepiol, B. *A new approach to the study of the α - σ phase transformation*. Hyperfine Interactions 126, 187 (2000).
- [Cieślak00b] Cieślak, J., Dubiel, S., and Sepiol, B. *Mössbauer effect study of the phase separation in the Fe-Cr system*. Journal of Physics: Condensed Matter 12, 6709 (2000).
- [Cieślak08a] Cieślak, J., Reissner, M., Dubiel, S., Wernisch, J., and Steiner, W. *Influence of composition and annealing conditions on the site-occupation in the sigma-phase of Fe-Cr and Fe-V systems*. Journal of Alloys and Compounds 460, 20 (2008).
- [Cieślak08b] Cieślak, J., Tobola, J., Dubiel, S., et al. *Electronic structure of a sigma-FeCr compound*. Journal of Physics: Condensed Matter 20, 235234 (2008).
- [Cook43] Cook, A. and Jones, F. *The Brittle Constituent of the Iron-Chromium System (Sigma Phase)*. J. Iron and Steel Inst. 148, 217 (1943).
- [Dubiel81] Dubiel, S. and Zukrowski, J. *Mössbauer Effect Study of Charge and Spin Transfer in Fe-Cr*. Journal of Magnetism and Magnetic Materials 23, 214 (1981).
- [Dubiel99] Dubiel, S., Cieślak, J., and Sepiol, B. *High-chromium ferritic steels*. Mössbauer Spectroscopy in Materials Science p. 107 (1999).
- [Elmer07] Elmer, J., Palmer, T., and Specht, E. *Direct observations of sigma phase formation in duplex stainless steels using in-situ synchrotron X-ray diffraction*. Metallurgical and Materials Transactions A 38, 464 (2007).
- [Greenwood71] Greenwood, N. and Gibb, T. *Mössbauer spectroscopy*. Chapman and Hall, London (1971).
- [Hansen58] Hansen, M., Anderko, K., and Salzberg, H. *Constitution of binary alloys*. Journal of the Electrochemical Society 105, 260C (1958).
- [Hennion83] Hennion, M. *Chemical SRO effects in ferromagnetic Fe alloys in relation to electronic band structure*. Journal of Physics F: Metal Physics 13, 2351 (1983).
- [Johnson39] Johnson, W. and Mehl, R. *Reaction kinetics in processes of nucleation and growth*. Trans. Am. Inst. Min. Metall. Eng. 135, 416 (1939).

- [Kolmogorov37] Kolmogorov, A. *On the statistical theory of the crystallization of metals*. Bull. Acad. Sci. USSR, Math. Ser 1, 355 (1937).
- [Kuwano85a] Kuwano, H. *Mössbauer effect study on the mechanism of the phase decomposition in iron-chromium alloys*. Transactions of the Japan institute of metals 26, 482 (1985).
- [Kuwano85b] Kuwano, H. *Mössbauer Effect Study on the Miscibility Gap of the Iron–Chromium Binary System*. Trans. Jpn. Inst. Met. 26, 473 (1985).
- [Lagarec98] Lagarec, K. and Rancourt, D. *Recoil, Mössbauer Spectral Analysis Software for Windows*. University of Ottawa, Canada (1998).
- [Lavrentiev07a] Lavrentiev, M., Drautz, R., Nguyen-Manh, D., Klaver, P., and Dudarev, S. *Monte Carlo study of thermodynamic properties and clustering in the bcc Fe-Cr system*. Physical Review B 75, 14208 (2007).
- [Lavrentiev07b] Lavrentiev, M., Nguyen-Manh, D., Drautz, R., Klaver, P., and Dudarev, S. *Monte Carlo simulations of Fe-Cr solid solution*. Scientific Modeling and Simulation 14, 203 (2007).
- [Massalski90] Massalski, T., Murray, J., Bennett, L., Baker, H., and Kacprzak, L. *Binary Alloy Phase Diagrams. Vol. 1*. ASM International, Materials Park, Ohio 44073, USA (1990).
- [Mirebeau84] Mirebeau, I., Hennion, M., and Parette, G. *First measurement of short-range-order inversion as a function of concentration in a transition alloy*. Physical Review Letters 53, 687 (1984).
- [Mittemeijer92] Mittemeijer, E. *Analysis of the kinetics of phase transformations*. Journal of Materials science 27, 3977 (1992).
- [Pfeiler07] Pfeiler, W. *Alloy physics: a comprehensive reference*. Wiley-VCH (2007).
- [Predel94] Predel, B. *Physical Chemistry Vol. 5, D, Cr-Cs ... Cu-Zr*. In O. Madelung (editor), *Landolt-Börnstein*. Springer-Verlag, Heidelberg (1994).
- [Rancourt91] Rancourt, D. and Ping, J. *Voigt-based methods for arbitrary-shape static hyperfine parameter distributions in Mössbauer spectroscopy*. Nuclear Instruments and Methods in Physics Research, Section B pp. 85–97 (1991).
- [Sluiter95] Sluiter, M., Esfarjani, K., and Kawazoe, Y. *Site Occupation Reversal in the Fe-Cr σ Phase*. Physical review letters 75, 3142 (1995).

Bibliography

- [Wegener66] Wegener, H. *Der Mössbauer-Effekt und seine Anwendungen in Physik und Chemie*. Bibliographisches Institut (1966).
- [Weißmantel95] Weißmantel, C. and Hamann, C. *Grundlagen der Festkörperphysik*. Johann Ambrosius Barth Verlag, Heidelberg-Leipzig, 4 edition (1995).
- [Yakel83] Yakel, H. *Atom distributions in sigma phases. I. Fe and Cr atom distributions in a binary sigma phase equilibrated at 1063, 1013 and 923 K*. Acta Crystallographica Section B: Structural Science 39, 20 (1983).

Curriculum vitae

Personal data

Name: Alice Mikikits-Leitner
Date of birth: August 31st, 1984
Place of birth: Vienna, Austria
Nationality: Austria
Marital status: Married

Education

1990–1994: Volksschule Wittelsbachstraße, Vienna
1994–2002: Bundesrealgymnasium Kleine Sperlgasse, Vienna
June 2002: Matura (school leaving examination) passed with distinction
2002– 2007: undergraduate studies (mathematics) at the Faculty of Mathematics, University of Vienna
June 2007: Mag. rer. nat. with distinction, University of Vienna
Diploma thesis: “Functional Analytic Methods for Hyperbolic Partial Differential Operators”,
Advisor: ao. Univ.-Prof. Günther Hörmann
2004 - 2009: undergraduate studies (physics) at the Faculty of Physics, University of Vienna
Sept. 2007 - present: PhD studies in mathematics at the University of Vienna

Positions

March 2007 - Feb. 2008: Teaching Assistant (Tutor), Faculty of Mathematics, University of Vienna
March 2008 - June 2008: Teaching Assistant (Tutor), University of Natural Resources and Applied Life Sciences (Boku), Vienna
Sept. 2007 - present: Research Assistent fully supported by the FWF START project Y330